Oct1 recruits the histone lysine demethylase Utx to canalize lineage specification

Jelena Perovanovic[1,3], Yifan Wu[1,3], Zuolian Shen[1,3], Erik Hughes[1,3], Mahesh B. Chandrasekharan[2,3], Dean Tantin[1,3,*]

[1]Department of Pathology
[2]Department of Radiation Oncology
[3]Huntsman Cancer Institute, University of Utah School of Medicine, Salt Lake City, UT 84112 U.S.A.

*Corresponding author
email: dean.tantin@path.utah.edu

Short title: Oct1 mediates lineage-specific gene activation

Keywords pre-implantation development; embryonic stem cells; mesoderm; single-cell RNA sequencing; Oct1/Pou2f1; Utx/Kmd3a; Smad3

Characters in title (including spaces): 82
Words in abstract: 157
Words main text: 4,562
Character count (including spaces): 56,952
Character count (excluding spaces): 48,701
Total main figures and tables: 7

Abstract

The pathways used by cells to transition between undifferentiated, pluripotent state and tissue-specific states are incompletely understood. Here we show that the widely-expressed transcription factor Oct1/Pou2f1 activates silent, developmental lineage-appropriate genes to "canalize" developmental progression. Using Oct1 inducible knockout embryonic stem cells, we show that that Oct1 deficiency impairs mesodermal and terminal muscle differentiation in a manner that can be rescued by Oct1 retroviral expression. Using bulk RNA-seq, we show that mesoderm-specific genes are not correctly induced early in the differentiation timecourse. Single-cell gene expression profiling reveals that Oct1-deficient cells lose coherence in temporal induction of lineage programs, and show inappropriate developmental lineage branching resulting in poorly differentiated cells state with epithelial characteristics and hallmarks of oxidative stress. In embryonic stem cells, Oct1 co-binds with Oct4 to genes critical for mesoderm induction. The Utx/Kdm6a histone lysine demethylase also binds to many of these genes, and using a prototypic *Pax3* gene we show that Oct1 recruits Utx to remove inhibitory H3K27me3 marks and activate expression. The specificity of the ubiquitous Oct1 protein for mesodermal genes can be explained by cooperative interactions with lineage-driving Smad transcription factors, as we show that Smad and Oct binding sites frequently coexist mesoderm-specific genes, that Oct1 and Smad3 interact, and that the sites and factors act cooperatively at the *Myog* enhancer. Overall, these results identify Oct1 as a key mediator of the induction of mesoderm lineage-specific genes.

Introduction

Lineage specification is a key process in the development of multicellular organisms by which undifferentiated cells progressively acquire tissue- and cell type-specific features (Seydoux and Braun, 2006). It is dynamically regulated, requiring extensive transcriptional and epigenetic remodeling to selectively activate lineage-appropriate gene expression programs and stably repress the expression of genes specific for alternative lineages. Embryonic stem cells (ESCs) represent a pluripotent cell type capable of both self-renewal and differentiation into all three embryonic germ layers (Beddington and Robertson, 1989). The three germ layers are established during gastrulation – a spatial reorganization of the embryo from a single-layer epiblast into the multilayered post-implantation embryo. One of the germ layers – mesoderm (MD) – gives rise to dermomyotome (muscle and dermis), sclerotome (axial skeleton) and lateral MD (cardiac) among other tissue types.

The transcriptional changes underlying lineage specification require extensive chromatin remodeling and spatiotemporal activation of genes encoding master transcription factors. Remodeling is potentiated by a unique chromatin landscape in pluripotent cells. Chromatin in ESCs is largely accessible and lacks stable heterochromatin domains (Meshorer and Misteli, 2006; Schlesinger and Meshorer, 2019). A large number of genes encoding lineage-specific developmental regulators are marked at promoters and gene bodies by covalently modified nucleosomes that simultaneously convey activating (H3K4me3) and repressing (H3K27me3) potential (Bernstein et al., 2006; Ku et al., 2008). In ESCs, these “bivalent” genes are silent or expressed at low levels, but lack DNA methylation and are poised for activation. During development, gene bivalency is thought to resolve via either removal of activating marks and gene silencing, or removal of repressive marks and gene activation. Which poised genes resolve in which direction is lineage-specific, resulting in distinct, cell fate-appropriate transcription programs and durable repression of lineage-inappropriate genes. However, the programs that instruct activation of the correct genes are poorly understood.

POU transcription factors play central roles in the regulation of development (Tantin, 2013). The well-known POU factor Oct4 (encoded by *Pou5f1*) is a master regulator of the induction and maintenance of pluripotency (Nichols et al., 1998; Palmieri et al., 1994; Takahashi and Yamanaka, 2006). Oct4 associates with bivalent genes in ESCs (Bernstein et al., 2006), but is silenced in their differentiated progeny before bivalency resolution and the induction of tissue- and cell type-specific gene expression (DeVeale et al., 2013). A second POU protein, Oct1, is co-expressed with Oct4, but unlike Oct4 is expressed beyond pluripotency (Shen et al., 2017). Oct1

84 is widely expressed and required for placental and embryonic development (Sebastiano et al.,
85 2010; V. E. H. Wang et al., 2004). Circumventing the placental defects via tetraploid
86 complementation results in developmental arrest at E8.25 with no more than five somites
87 (Sebastiano et al., 2010). Oct1-deficient ESCs are morphologically normal and proliferate and
88 self-renewal normally, but upon differentiation show phenotypic and gene expression defects
89 including decreased developmental lineage-specific gene expression and elevated expression of
90 developmentally incorrect genes (Shen et al., 2017). Extended incubation of these cells supports
91 an interpretation that there is a failure to differentiate rather than a simple kinetic delay (Shen et
92 al., 2017). The underlying molecular mechanisms by which Oct1 regulates lineage differentiation
93 are unknown.

94 Here, using MD differentiation of *Oct1*/*Pou2f1* inducible-conditional ESCs, we show that
95 pluripotent cells lacking Oct1 fail to form terminally differentiated myotubes. Differentiation is
96 restored by Oct1 retroviral complementation. Bulk RNA-seq profiling early in the differentiation
97 timecourse identifies gene expression abnormalities early in MD differentiation that predict the
98 later phenotypic defects. Single-cell RNA sequencing reveals that cells lacking Oct1 accumulate
99 abnormal cell populations associated with epithelial characteristics, oxidative stress and early
100 MD, while almost completely failing to reach somite-stage differentiation. Pseudotime analysis
101 reveal increased predilection to proceed down incorrect developmental trajectories, and "fuzzy"
102 differentiation programs. We show that Oct1 interacts with components of the Utx (Kdm3a)
103 H3K27me3 demethylase complex, and recruits Utx to developmentally appropriate target genes.
104 At tested targets this results in specific removal of H3K27me3 and de-repression. Binding sites
105 for Oct1 and Oct4 in pluripotent cells in which Oct1 binding is carried forward during MD
106 differentiation are also enriched in sites for Smad transcription factors, key mediators of MD
107 specification. Oct1 and Smad3 interact in differentiating cells, providing a means of restricting
108 Oct1's activating potential to MD-specific genes. The cumulative results support a model in which
109 Oct1 "canalizes" differentiation by supporting the induction of lineage-specific genes.

Results

Loss of Oct1 causes aberrant mesodermal differentiation

To study the consequences of Oct1 deficiency for MD development, we differentiated Oct1 inducible-conditional *Pou2f1*$^{fl/fl}$;Rosa26-CreER^{T2};LSL-YFP control ESCs (hereafter, "parental" cells) and derived tamoxifen-treated, Oct1-deficient cells (Shen et al., 2017) (hereafter, "cKO") using an MD differentiation protocol that results in differentiated myotubes after 10 days of culture. The differentiation process is initiated by Bmp4 treatment to activate TGFβ signaling, and generates dynamic changes in metabolic programs (Oginuma et al., 2017), epithelial-to-mesenchymal transition (EMT) (Diaz-Cuadros et al., 2020) and induction of MD-specific gene expression programs during the differentiation timecourse (Chal et al., 2015). Parental cells were differentiated for 11 days (D11) to generate early myotubes to identify changes in myotube structure. Immunostaining for embryonic myosin heavy chain (MyH-emb) reveals robust expression in fused myotubes in parental cells, with cKO expression close to background (Figure 1A). We then queried expression of myogenic genes (*Myod* and *Myog*) using more fully differentiated parental and cKO cells (D19) and RT-qPCR. Relative to Rps2 (which encodes a ribosomal 40S subunit), both genes were strongly expressed in parental but not cKO cells (Figure 1B). These results demonstrate that cKO ESCs differentiate into muscle poorly, consistent with their defective early gene expression programs and developmental trajectories.

To determine the effect of ectopic Oct1 expression, we transduced parental and cKO ESCs with retroviral vectors encoding murine Oct1, or empty vector (EV) controls. The vectors encode a puromycin resistance cassette, allowing for selection of transduced cells. Immediately after selection, populations of transduced cells were subjected to MD differentiation to D11, and tested for *Myod*, *Myog* and *Pax3* by RT-qPCR. Differentiating cKO ESCs transduced with Oct1 but not empty vector expressed *Myod* and *Myog* more strongly. *Pax3* expression by contrast was reduced (Figure 1C). The combination of elevated *Myod* and *Myog* with diminished *Pax3* expression at late differentiation timepoints suggests that restoration of Oct1 allows cells to more efficiently transit through a *Pax3*-expressing intermediate state, such that more cells enter into a terminal myogenic program. Interestingly retrovirally expressed ectopic Oct1 expression also improved differentiation outcomes using parental cells (Figure 1C). Immunoblotting confirmed ectopic Oct1 expression and complementation of Oct1 deficiency (Figure 1D).

Defective lineage-appropriate gene expression differentiating Oct1-deficient cells

142 To identify how Oct1 loss perturbs MD differentiation, we performed bulk RNA-seq using parental
143 and Oct1 cKO cells. Three replicates were performed per condition. ~1700, ~800 and 3,300
144 significantly differentially expressed genes were identified at D0, D3 and D6, respectively (FDR ≤
145 0.05; -1 < log2FC < 1, Supplementary Table 1). Euclidean distance analysis reveals tight
146 correlations between replicates and conditions at D0 and D3, but divergence at D6 relative to the
147 other conditions, and devergence between parental and cKO D6 replicates (Supplemental Figure
148 1). Unsupervised hierarchical clustering reveals groups of genes regulated similarly between
149 parental and cKO cells, and others with differential expression (Figure 1E). Cluster 2 for example
150 shows strong induction in differentiating parental but failed induction in cKO D6 cells. Example
151 genes in this set include *Pax3*, *Pax7* and *Myog* (Figure 1E, box). GO analysis of the differentially
152 expressed genes in cluster 2 reveals association with differentiation to neural tube
153 (neuroectoderm) and somite (Figure 1F). By contrast, clusters 1 and 4, which were associated
154 with aberrant gene expression in differentiating cKO cells, were associated with lineage-
155 inappropriate terms such as primordial germ cells, vascular system and stromal cells (Figure 1F
156 and not shown). To identify potential regulators of cluster 2 genes with failed induction in
157 differentiating cKO cells, we queried the ChIP Enrichment Analysis (ChEA) database (Lachmann
158 et al., 2010). Cluster 2 genes tend to be bound by the polycomb repressor compex 2 (PRC2)
159 components Suz12 and Mtf2 (Figure 1F). Example tracks are shown in Figure 4D for *Pou5f1*
160 (pluripotency), *Tbxt* (*T*/*Brachyury*, cluster 3) and *Pax7* (cluster 2). The retained D3 expression of
161 *Pou5f1*, which encodes Oct4, provides a likely explanation for the tight correlations between gene
162 expression states at D0 and D3 with divergence at D6 (Supplemental Figure 1), as the cells
163 maintain pluripotency characteristics through D3. These data indicate that Oct1 loss results in
164 defective induction of developmental genes that are also regulated by chromatin-modifying
165 activities that act on H3K27me3.
166
167 **Differentiating ESCs lacking Oct1 proceed down abnormal developmental trajectories**
168 To investigate perturbations in cell populations and gene expression at single-cell resolution, we
169 performed single-cell RNA-seq (scRNA-seq) using parental and cKO ESCs, and cells
170 differentiated towards MD for 3 or 6 days. Cell numbers ranged between 1000 and 2500, with
171 reads per cell ranging between 90,000 and 200,000 (see methods). Data from the different
172 conditions were subjected to graph-based clustering and uniform manifold approximation and
173 projection (UMAP) to visualize clusters of cells with similar gene expression. Integrated analysis
174 of undifferentiated parental ESCs and parental cells at the two differentiation timepoints identifies

175 a range of expected cell populations, from naïve and primed pluripotency to neuromesodermal,
176 paraxial MD and early somite (Figure 2A). These populations recapitulate developmental stages
177 associated with induction of markers associated with early MD (*Fgf17* and *Tbxt*/*T*/*Brachyury*;
178 cluster 2 and 7), neuromesoderm (*Hoxc9*, *Pax3*, *Sox2*), paraxial MD (*Meox1*, *Twist1*, *Pax3*) and
179 early somite and neuronal progenitors (*Cxcr4, Uncx*) (Figure 2B, Supplementary Figure 2 and not
180 shown). These results provide a single cell-resolution map of early MD differentiation.

181 Next, we compared the parental controls to cKO cells to identify changes in cell
182 populations and gene expression. D0 and D3 cKO cells show few differences from parental, Oct1
183 sufficient cells (Supplementary Table 2). In contrast, D6 cKO cells show poor differentiation
184 capacity with reductions in key mesodermal clusters (Figure 2C). For example, populations
185 characterized by neuromosodermal and paraxial MD gene expression represent the largest two
186 parental cell clusters, accounting for 14.7 and 12.9% of cells, respectively, while populations
187 associated with blood progenitors and somites account for 5.7% and 5.6% of cells (Figure 2C, left
188 panel). The complexity in the populations is consistent with findings that somites are derived from
189 multiple transcriptional trajectories including early paraxial mesoderm and neuromesodermal
190 progenitors (Guibentif et al., 2021). In contrast, cKO D6 cells show increases in clusters that retain
191 epithelial characteristics and dramatically decreased percentages of neuromesodermal
192 progenitors (2.3%, a six-fold decrease), paraxial MD (7.5%, two-fold), and both blood progenitors
193 (1.1%, >5-fold) and somites (0.5%, >10-fold, Figure 2C, right panel). This failure to produce more
194 differentiated MD lineage cells is consistent with findings that ESCs lacking Oct1 differentiate
195 poorly into myotubes (Figure 1A).

196 Gene expression comparisons between parental and cKO paraxial mesoderm clusters
197 reveals that cKO cells fail to robustly induce lineage-appropriate genes such as *Pax3* and *Pax7*,
198 and inappropriately upregulate lineage-inappropriate markers such as the epithelial-specific
199 genes *Krt8* and *Krt18* (Figure 2D). These results show that Oct1 is necessary for accurate
200 mesoderm differentiation and to suppress expression of genes for alternative lineages.

201 Pseudotime analysis of scRNA-seq data allows multiple differentiation timepoints to be
202 overlaid with defined starting (ESC) and endpoint (somite) populations. Parental control cells
203 progress through a largely linear pathway with one minor branch retaining an inappropriate
204 epithelial fate (Figure 3A, top panel). In contrast, differentiating cKO ESCs show a larger
205 proportion inappropriate branching into alternative developmental trajectories (bottom panel),
206 consistent with the diminished developmental progression of paraxial MD to the somite stage,
207 and consistent with enrichment of cells that inappropriately maintain an epithelial state (Figure 2C

208 and Supplementary Figure 2). We also examined pseudotemporal gene expression using specific
209 genes associated with pluripotency and MD development. In this analysis, the position of each
210 cell in pseudotime is shown on the X-axis and the degree of expression for the indicated gene on
211 the Y-axis (Figure 3B). Parental cells show robust early expression of genes associated with
212 pluripotency such *as Klf4* that lose expression roughly mid-way through pseudotime. *Tbxt* is
213 transiently induced, while the early somite markers *Pax7* and *Cxcr4* are efficiently and
214 coordinately induced later (Figure 3B, top panel). In contrast, cKO cells exhibit inappropriately
215 prolonged expression of *Klf4* and *Tbxt*, and largely fail to upregulate *Pax7* and *Cxcr4* (bottom
216 panel). We used pseudotemporal ordering to visualize expression of the 2000 most variable
217 (dynamic) genes in parental cells, and compared expression of the same genes in the same order
218 in cKO cells (Figure 3C). This analysis revealed clusters associated with pluripotency (*Klf4*,
219 *Nanog, Pou5f1*), early MD differentiation (*T*), paraxial mesoderm (*Rspo3, Meox1*), and early
220 somites (*Dll1, Pax3*). The pseudotime gene expression pattern for cKO cells revealed largely
221 normal expression of early gene expression markers, but loss of temporal coherence at
222 subsequent steps. These "fuzzy" patterns of gene expression begin early in differentiation, with
223 for example prolonged expression of genes such as *Tbxt* and noncoherent expression of genes
224 associated with paraxial mesoderm such as *Meox1* and *Rspo3*. The diffuse pattern is different
225 from what would be expected with a kinetic delay, which would cause a rightward shift. In addition,
226 the induction of somitic genes normally expressed later in development such as *Dll1*, *Pax3* and
227 *Pax7* was poor in cKO cells (Figure 3C).

228 RNA velocity analysis allows developmental directionality to be inferred relative to other
229 cells by comparing the ratio of unspliced, newly-synthesized pre-mRNA to mature spliced mRNA.
230 A vector is then assigned to each cell that indicates developmental direction and magnitude
231 relative to the other cells. We clustered the cells separately by genotype, resulting in different
232 patterns between genotype and compared to cells clustered together (Figure 3D). Applying
233 velocity to this clustering, we found that D6 differentiated parental cells form discrete clusters with
234 dynamic developmental progression, e.g. paraxial MD and somite (Figure 3D, marked by long
235 arrows). cKO cells by contrast are marked by stationary profiles indicative of failed differentiation
236 potential, with cells progressing primarily towards a poorly differentiated state characterized by
237 an aberrant epithelial state and multiple lineage markers (Figure 3D, epithelial clusters).
238 Cumulatively, the data demonstrate that Oct1 is required for efficient early adoption of the MD
239 differentiation program, with Oct1-deficient cells unable to canalize appropriate lineage
240 specification programs.

241

242 **Oct1 occupies developmental genes in ESCs**

243 One model that explains the above data is that Oct1 occupies developmental-specific targets
244 bound by Oct4 in ESCs, to mediate induction of developmentally appropriate genes and
245 repression of genes specific to alternative lineages. To test this hypothesis, we performed
246 chromatin immunoprecipitation (ChIP-seq) using antibodies against Oct1 and Oct4. Prior work
247 showed that Oct1 occupancy at Oct4 targets increases during retinoic acid (RA)-mediated
248 differentiation when Oct4 expression is lost (Shen et al., 2017). RA ultimately differentiates cells
249 into neuroectodermal lineages (Bain et al., 1995). In undifferentiated ESCs, strong Oct1 binding
250 (with Oct4) was only observed in a group of ~100 genes containing Oct protein variant binding
251 sites termed MOREs (More-palindromic Octamer Recognition Element) (Shen et al., 2017). We
252 used a different Oct1 antibody with superior enrichment properties (see methods) to perform
253 ChIP-seq with undifferentiated parental Oct1-sufficient ESCs, as well as cells differentiated
254 towards MD for 3 or 6 days. Oct4 ChIP-seq in undifferentiated ESCs was performed as a parallel
255 control.

256 In pluripotent cells, ~22,000 Oct4 peaks were identified, corresponding to ~6,000 genes
257 with transcription start sites (TSS) within 20 kb (Supplementary Table 3). ~45% of Oct4 targets
258 directly overlap Oct1 peaks. Conversely ~60% of Oct1 targets overlap Oct4 peaks (Figure 4A),
259 indicating substantial overlap between binding of the two transcription factors. Shared Oct1/Oct4
260 targets in ESCs include *Polr2a*, which encodes the largest subunit of RNA polymerase II, *Pou5f1*,
261 which encodes Oct4, and *Dll1*, which encodes a developmentally-inducible mediator of Notch
262 signaling expressed in the MD lineage where it regulates muscle development (Zhang et al.,
263 2021). Undifferentiated (D0) Oct4 and Oct1 binding tracks are shown in Supplementary Figure 3.
264 We also confirmed Oct1 and Oct4 binding to *Polr2a*, *Pou5f1* and *Dll1* using ChIP-qPCR
265 (Supplementary Figure 3). Oct1 binding to *Polr2a*, which contains two adjacent MOREs that can
266 bind four Oct proteins (Kang et al., 2009a), is exceptional relative to other genes in that it is far
267 stronger than Oct4 (100× stronger for *Polr2a*, 3-10× weaker for *Pou5f1* and *Dll*). Re-ChIP
268 (sequential ChIP) indicates that Oct1 and Oct4 bind these sites simultaneously. The signal was
269 lost in Oct1 cKO ESCs, indicating specificity for Oct1 (Supplementary Figure 3). Cumulatively, the
270 data indicate that in ESCs Oct1 co-binds with Oct4 to an array of targets, including developmental-
271 specific targets.

272 We then performed ChIP-seq using D3 and D6 MD-differentiated cells. Only 199 Oct4-
273 bound peaks not occupied by Oct1 in pluripotent cells become occupied by Oct1 at D6 of MD

274 differentiation (Figure 4A). In contrast, 807 shared Oct4/Oct1 peaks in pluripotent cells continue
275 to be bound by Oct1 at D6. Analysis of these peaks using GREAT (McLean et al., 2010) identifies
276 enrichment for oxidative stress, ribosomal and mitochondrial organization, Notch signaling and
277 post-implantation development including somite formation (Supplementary Figure 4A).
278 Additionally, >6000 peaks become uniquely bound by Oct1 at MD D6 (Figure 4A). >2300 peaks
279 are uniquely bound at D3 (Supplementary Figure 4B).

280 To pattern Oct1 and Oct4 occupancy during MD differentiation, we applied hierarchical
281 clustering. Three major clusters of occupied targets were identified, two of which show decreased
282 or static Oct1 binding over time (Figure 4B, clusters 1 and 2). Gene ontogeny (GO) analysis
283 indicates involvement in signaling, mitochondrial function, stem cell differentiation and the
284 regulation of Notch and TGFβ signaling. Oct1 and Oct4 enrichment at a cluster 1 gene encoding
285 a pluripotency factor (*Pou5f1*) and two cluster 2 genes encoding MD/myogenic transcription
286 factors (*Pax3* and *Myog*) is shown in Figure 4C. We also queried Oct1 binding to genes associated
287 with bivalency, which can be used as a surrogate for silent, poised developmental genes. To
288 identify bivalent genes, we intersected ESC H3K27me3- and H3K4me3-enriched ChIP-seq peaks
289 from the ENCODE database. This procedure identifies 3861 bivalent genes (Supplementary
290 Table 4). To query Oct1 occupancy on these genes during differentiation, we intersected the
291 bivalent gene dataset with Oct1 ChIP-seq in pluripotent and MD-differentiated parental cells,
292 observing an increase in binding over time (Figure 4D, green and blue lines). A similar analysis
293 at D6 using just MD-specific bivalent genes (generated by intersecting the bivalent gene dataset
294 with MD development GO:0007498, Supplementary Table 5) shows even stronger Oct1
295 enrichment (Figure 4D, purple line). These findings indicate that Oct1 robustly binds to bivalent
296 genes both in pluripotent cells and their differentiated progeny, with binding increasing at lineage-
297 specific genes during differentiation.

298 In contrast, Oct1 binding in Figure 4B increases with differentiation in cluster 3. GO
299 analysis indicates that genes near these peaks are associated with chromatin-modifying activities
300 including histone acetyltransferase and polycomb group complexes. Oct1 and Oct4 enrichment
301 at example cluster 3 genes encoding polycomb complex members (*Ezh2*, *Suz12*, *Ring1* and
302 *Ezh1*) is shown in Supplementary Figure 5A. These genes show a gain in Oct1 occupancy as
303 cells progress from pluripotency through D3 to D6 of MD differentiation. In the scRNA-seq UMAP
304 projection, *Ezh2* expression is downregulated in cKO cells at D6, in particular in paraxial
305 mesoderm (Supplementary Figure 5B-D). These data indicate that during MD differentiation, Oct1

306 directly binds to, and mediates the induction of, genes encoding epigenetic regulators associated
307 with H3K27me3.
308
309 **Oct1 Recruits Utx to the *Pax3* Target Gene to Remove H3K27me3.** Lineage-appropriate
310 poised developmental genes become activated in part via the removal of repressive H3K27me3
311 marks (Bernstein et al., 2006; Dhar et al., 2016a). Our findings indicate that genes with failed
312 induction in differentiating cKO cells tend to be bound by chromatin-modifying complexes that act
313 on H3K27me3 (Figure 1F). We hypothesized that Oct1 locally recruits H3K27-specific
314 demethylases to lineage-specific genes to mediate their induction during differentiation. One such
315 demethylase is Utx/Kdm6a (Cloos et al., 2008), which has been shown to regulate MD
316 differentiation (Wang et al., 2012). To test the association between Oct1 binding and Utx, we also
317 performed ChIP-seq using H3K27me3 and Utx antibodies at D6 of differentiation of parental, Oct1
318 sufficient cells. ~12,000 H3K27me3 peaks and ~12,000 Utx peaks were identified, corresponding
319 to ~11,000 genes within 20 kb (Supplementary Table 3). Unsupervised hierarchical clustering
320 together with Oct1 peaks from the same cells identifies shared and distinct peaks, including weak
321 Oct1 binding events with strong Utx and H3K27me3 association (Figure 5A, cluster 3), and strong
322 Oct1 binding events associated with weaker Utx and lack of H3K27me3 (cluster 4). This latter
323 cluster includes genes induced in MD such as *Pax3, Pax7* and *Myog*. We interpret cluster 3 to be
324 developmental genes that remain poised at this timepoint, and cluster 4 to be lineage-appropritate
325 genes that have been activated. GO terms associated with these clusters were enriched for
326 development and musculoskeletal abnormalities (Figure 5B). Intersecting the Utx and Oct1 ChIP-
327 seq peaks identifies a high degree of overlap, with ~70% of Oct1-bound peaks also associating
328 with Utx (Figure 5C).
329 To test if cKO cells inappropriately retain H3K27me3 at lineage-appropriate genes during
330 MD differentiation, we performed ChIP-qPCR using primers flanking a strong Oct1 peak on the
331 *Pax3* promoter. *Pax3* is induced by D6 of MD differentiation, and reduced in Oct1 cKO cells at
332 this timepoint (Figure 1E and Figure 3C). As expected, H3K27me3 was robust and equivalent in
333 parental and cKO D0 undifferentiated cells. D6 parental cells showed reduced H3K27me3, while
334 in contrast, cKO cells inappropriately retained elevated H3K27me3 (Figure 5D). This failure to
335 remove H3K27me3 resulted in ~3-fold higher H3K27me3 enrichment in differentiated cKO relative
336 to parental cells. Global H3K27me3 levels are unchanged at the same timepoint, as evidenced
337 by immunofluorescence (Figure 5E). Next, we performed Utx ChIP-qPCR with the same primers.
338 Utx is enriched at the *Pax3* promoter at D6 of MD differentiation, validating the ChIP-seq

339 enrichment in parental cells. Further, Utx showed reduced enrichment in cKO cells (Figure 5F).
340 These results indicate association of Utx and Oct1 at *Pax3*, and specific defects in removing
341 H3K27me3 from *Pax3* in differentiating Oct1-deficient cells.
342 We then determined if Oct1 and Utx interact using extracts from undifferentiated and D6-
343 differentiated parental ESCs and co-immunoprecipitation. The Oct1-Utx interaction is present
344 even in ESCs, and is maintained during differentiation (Figure 5G). These results support the
345 interpretation that Oct1 interacts with Utx and recruits it to target genes during differentiation to
346 help mediate their activation. Utx recruitment by Oct1 potentially explains the failed induction of
347 lineage-appropriate genes such as *Pax3*, and the failed removal of H3K27me3 in cKO cells
348 (Figure 5D). Oct1, Oct4 and Utx binding to *Pax3* is shown in Figure 5H.
349
350 **Oct1 interacts with Smad3, and cooperates with Smad proteins at *Myog* in cells**
351 **differentiating towards MD.** The broad expression of Oct1 raised the question of how Oct1
352 mediates gene activation specifically at MD lineage-specific. Chromatin accessibility, lineage-
353 specific signaling and co-bound transcription regulators may provide this specificity. We
354 performed motif analysis (Heinz et al., 2010) using DNA sequences ±100 bp from the center of
355 the 807 peaks co-bound by Oct1 and Oct4 in pluripotent cells that remain Oct1-bound during MD
356 differentiation (Figure 4A). This procedure identifies not only Oct1 sites, but also binding sites for
357 Smads, the terminal transcription regulators of TGFβ/Nodal/BMP signaling (Figure 6A). TGFβ
358 signals and downstream Smad transcription factor activity are critical for MD induction (Conlon et
359 al., 1994; Zhou et al., 1993). A study identified Oct1 transcription factor motifs near binding events
360 for zebrafish Smad2/3 and further showed that ectopic expression of the zebrafish Oct1 ortholog
361 enhances mesoderm induction, that zebrafish Smad2 and Oct1 physically interact, and that the
362 two factors cooperate to enhance transcription (Liu et al., 2011). Mammalian Smad3 also interacts
363 with Oct4 and co-occupies target genes in pluripotent cells (Mullen et al., 2011). Consistent with
364 these findings, Oct1 antibodies efficiently co-precipitate Smad3 in D6 MD-differentiated cells
365 (Figure 6B). *Smad3* is expressed in undifferentiated parental populations, but further induced by
366 MD differentiation (Figure 6C).
367 To gain more insight into mechanism, we tested if Oct1 and Smad proteins synergize to
368 regulate gene expression. We cloned an 85 bp region ~3 kb upstream of the *Myog* gene together
369 with the CMV core promoter upstream of a luciferase reporter vector (Figure 6D). This region
370 contains two octamer sites and two Smad sites, and overlaps with an ENCODE distal enhancer

371 signature (Abascal et al., 2020). The region is also located within a known super-enhancer
372 associated with myotubes (Hnisz et al., 2013). The sequences were inserted into a reporter vector
373 that expresses secreted nanoLuciferase, and co-transfected with a plasmid constitutively
374 expressing secreted mCherry (Wider and Picard, 2017) as an internal standard into MEFs lacking
375 Oct1 (Victoria E. H. Wang et al., 2004) (Figure 6D). Cells were either co-transfected with a
376 construct encoding mouse Oct1, treated with recombinant TGFβ1, or both. The two treatments
377 together generate cooperative luciferase activity (Figure 6E). No such activity was observed using
378 constructs with mutant Oct/Smad binding sites. These results indicate that Oct and Smad sites at
379 the *Myog* enhancer cooperate to drive gene expression.
380

381 **Discussion**

382 During development, chromatin transitions from a pluripotent state permissive for different
383 lineages to a lineage-restricted state. Pluripotent cells maintain genes encoding developmental-
384 specific mediators in a poised configuration that allows for later induction or stable repression,
385 depending on the developmental lineage (Bernstein et al., 2006). Oct1-deficient animals manifest
386 defective induction of MD-derived somites, cardiac tissue and blood cells (Sebastiano et al., 2010;
387 V. E. H. Wang et al., 2004). The co-expression of Oct1 with Oct4 in pluripotent cells and
388 maintenance of Oct1 beyond Oct4 silencing (Shen et al., 2017), together with the severe
389 developmental phenotype of Oct1 null animals, prompted us to study the role of Oct1 during
390 differentiation into the MD lineage. Here we show that Oct1-deficient ESCs manifest defective MD
391 differentiation, including failure to express *Myod* and *Myog* mRNA, and myosin heavy chain
392 protein. During mesodermal differentiation, Oct1 continues to bind developmental lineage-specific
393 genes co-bound with its paralog Oct4 in pluripotent cells. Further, Oct1 helps mediate the
394 induction of the subset of MD lineage-specific. We show that Oct1 and Utx binding events
395 significantly overlap, that Oct1 interacts with Utx and that Oct1 localizes Utx to a MD-specific
396 target to remove repressive H3K27me3 marks. Specificity is achieved at least in part through
397 cooperative interactions with Smad proteins, known drivers of MD induction. Because Oct1 is
398 widely expressed and results in defective differentiation into multiple lineages (Shen et al., 2017),
399 we anticipate that this mechanism may act widely, with the only unique aspect being the
400 association with lineage-driving transcription regulators such as Smad proteins in the case of MD.

401 The central role of Oct1 in "canalizing" differentiating pluripotent cells in early steps of
402 mesodermal specification was shown using single-cell RNA-seq with Oct1 cKO ESCs. In the
403 absence of Oct1, cells undergoing differentiation retain an epithelial state, and achieve
404 neuromesodermal and somite-stage gene expression patterns poorly and in reduced numbers.
405 Increased populations of cells appear associated with oxidative stress, consistent with findings
406 that cells lacking Oct1 have elevated reactive oxygen species levels (Tantin et al., 2005). cKO
407 cells mis-express developmentally inappropriate genes and undergo inappropriate developmental
408 branching towards poorly differentiated states marked by epithelial gene expression and oxidative
409 stress. Unlike the expected effect of loss of lineage-specific master regulators where cell fate
410 often shifts to a specific alternate lineage, these cells lack clear lineage signatures. The induction
411 of genes important early in MD differentiation such as *Tbxt* becomes weaker and loses temporal
412 coherence. Later, there is failed induction of genes such as *Pax7* and *Cxcr4*.

413 In MD-differentiating cells, Oct1 occupies a subset of genes bound by Oct4 in pluripotent
414 cells. These include lineage-specific developmental mediators and genes encoding chromatin-
415 modifying enzymes. Oct1 occupancy on these genes increases with differentiation, suggesting a
416 critical role in canalization of cell fate. We find that Oct1 recruits Utx to lineage-specific, Oct1-
417 bound targets such as *Pax3*. The lack of Utx recruitment to lineage-specific genes in cKO cells is
418 consistent with the abnormal retention of H3K27me3 at the promoter and the failed transcriptional
419 upregulation. No global changes in H3K27me3 were observed, consistent with recruitment by
420 Oct1 to mediate focal removal (Wang et al., 2012). An "anti-repression" mechanism for Oct1
421 involving the removal of repressive chromatin marks has been described for Oct1 before, for
422 H3K9me2 (Shakya et al., 2011). To our knowledge this is the first description of a role for Oct1
423 and K3K27me3. Loss of Utx allows for maintainance of an undifferentiated state, but interferes
424 with MD differentiation (Dhar et al., 2016b).
425 One mechanism that allows Oct1 to gain specificity for MD-appropriate targets is
426 collaboration with Smad3. Smad transcription factor binding sites are enriched near sites of Oct1
427 binding during MD differentiation. TGFβ signals drive Smad transcription factor binding and are
428 critical for MD specification (Liu et al., 2011; Mullen et al., 2011). Co-IP experiments in D6 MD-
429 differentiated cells show an interaction between Oct1 and Smad3, consistent with prior findings
430 in zebrafish (Liu et al., 2011). A model for Oct1's function at lineage-specific genes during MD
431 specification and later differentiation is shown in Figure 7. In this model, Oct1 and Smad form
432 cooperative complexes at MD-specific genes, and Utx recruitment to Oct1 allows for loss of the
433 repressive H3K27me3 mark and gene activation. Subsequently, other transcription factors (e.g.,
434 MyoD) act as primary "on" switches to induce gene expression. Oct1 also binds and induces the
435 expression of genes encoding PRC complex members such as *Ezh2* in MD-specific clusters in
436 parental but not cKO cells. The increased expression of PRC components may solidify lineage
437 specification by aiding the repression of the large number of genes specific to alternative lineages
438 (Collinson et al., 2016).
439 Under MD differentiation conditions, exogenous Oct1 increases expression of the terminal
440 differentiation markers *Myod* and *Myog*, while decreasing the early lineage-specification marker
441 *Pax3*, which is transiently expressed during MD differentiation and is necessary for later
442 expression of myogenic genes. Because *Pax3* is no longer expressed in terminally differentiating
443 cells, these results suggest that ectopic Oct1 may enable transit through a *Pax3*-expressing
444 intermediate to potentiate productive terminal differentiation. More investigation into this pathway

445 is necessary to test if Oct1 can be used to more efficiently differentiate pluripotent cells. Such
446 improvements could have implications for regenerative medicine.

447 **Figure Legends**

448

449 **Figure 1. Failed MD/muscle lineage induction in differentiating Oct1 cKO ESCs.** (**A**)
450 Embryonic myosin heavy chain (MyHC-emb) expression alone and merged with DAPI is shown
451 using parental (top panel) or cKO (bottom panel) cells at MD differentiation D11. (**B**) Relative
452 mRNA expression levels of the myogenic genes *Myod1* and *Myog* in parental and cKO ESCs
453 differentiated for 19D. Data represent an average of biological triplicates. Error bars depict ±SEM.
454 (**C**) RT-qPCR for the myogenic genes *Myod1*, *Myog* and *Pax3* in parental and cKO cells
455 transduced with retroviruses encoding Oct1 or empty vector. Transduced cells were selected
456 using puromycin for 48 hr prior to differentiation for 11D. Empty vector values were set to 1. Data
457 represent an average of biological triplicates. Error bars depict ±SEM. (**D**) Immunoblot showing
458 ectopic Oct1 expression in parental and cKO cells. β-actin is shown as a loading standard. (**E**)
459 Bulk RNA-seq heatmap of differentially expressed genes (parental vs. cKO) at D0, D3 and D6 of
460 MD differentiation is shown. Cluster 2 shows poor gene induction in the Oct1-deficient condition.
461 Representative cluster 2 genes are shown at right. (**F**) Jensen Tissue and ChIP-X Enrichment
462 Analysis (ChEA) query results for Cluster 2 in (B) are shown. (**G**) Example RNA-seq genome
463 tracks (*Pou5f1*, *Tbxt*, *Pax7*) are shown. *Pax7* is an example cluster 2 gene. Y-axes were group-
464 autoscaled for each gene.

465

466 **Figure 2. Differentiating Oct1-deficient ESCs canalize poorly into mesodermal lineages.** (**A**)
467 UMAP projection of scRNA-seq data from superimposed parental (Oct1 sufficient)
468 undifferentiated ESCs, and parental cells early during MD differentiation (days 3 and 6). Clusters
469 of cells were labeled based the expression of developmental markers as in (B). MD-associated
470 clusters are shown in bold. Three combined replicate plates were used for the analysis. (**B**) Violin
471 plots showing gene expression levels of key developmental markers by cluster. Data were log-
472 normalized for each cell using the natural logarithm, scaled and averaged using mean(expm1(x)).
473 (**C**) Comparative UMAP projections of integrated D6 parental and Oct1-deficient (cKO) scRNA-
474 seq populations. Clusters were labeled computationally and identified based on gene expression.
475 Relative frequencies are shown. MD lineage-associated clusters are shown in bold. (**D**)
476 Differential gene expression analysis of the neuromesodermal cluster shown as a scatter plot.
477 Red dots depict significantly differentially expressed genes based on FDR corrected $p < 0.05$ and
478 fold change >1.2. Example differentially expressed genes are labeled.

479

480 **Figure 3. Oct1-deficient cells show perturbed developmental trajectories.** (**A**) Pseudotime
481 analysis of pluripotent and differentiating parental (top panel) and cKO (bottom panel) cells.
482 Colors correspond to the time point at which cells were collected (red: D0, green: D3, blue: D6).
483 (**B**) *Klf4*, *Tbxt*, *Pax7* and *Cxrc4* mRNA expression across pseudotime in parental (top panels) and
484 cKO (bottom panels). Black trendline represents an average expression for a given gene across
485 all populations. (**C**) Heatmap depicting expression of the 2000 most dynamically expressed genes
486 (based on FindVariableFeatures function, Seurat) in parental D6 cells. Gene expression was
487 plotted as a heat map across pseudotime in parental (left panel) and cKO (right panel). Dynamic
488 genes were first hierarchically clustered in parental cells to cluster groups of genes that behave
489 similarly in pseudotime, then plotted in the same order in cKO cells. (**D**) Velocity gene expression
490 analysis of parental (left panel) and cKO (right panel) cells at differentiation day 6. Arrows point
491 toward cells with gene expression closest to the future state of each cell based on
492 unspliced/spliced transcripts. Arrow length represents magnitude. Clusters in bold are associated
493 with MD differentiation.

494

495 **Figure 4. Oct1 co-occupies target sites with Oct4 in ESCs, and regulates their expression**
496 **during differentiation.** (**A**) Venn diagram showing common and unique Oct4 and Oct1 binding
497 sites based on ChIP-seq in parental ESCs and at D3 and D6 of mesodermal differentiation. (**B**) A
498 matrix of Oct4 and Oct1 ChIP-seq enrichment 2 kb around peak centers was computed for the
499 merged peak list and shown as heatmap. Positions in color show high enrichment and white
500 shows no enrichment. (**C**) Example cluster 1 and 2 genome tracks: *Pou5f1* (cluster 1), *Pax3*
501 (cluster 2) and *Myog* (cluster 2). (**D**) Oct1 enrichment based on tag density at peak center at
502 annotated bivalent genes in ESCs (red), and at MD differentiation D3 and D6 (green and blue).
503 An additional analysis was performed for MD-specific bivalent genes at MD differentiation D6
504 (purple).

505

506 **Figure 5. Oct1 recruits Utx to demethylate H3K27me3 at lineage-appropriate genes.** (**A**)
507 Oct1, H3K27me3 and Utx ChIP-seq enrichment 2 kb around peak centers was computed for the
508 merged peak list and shown as heatmap. (**B**) Human Phenotype Ontology terms for Cluster 3 and
509 4 genes from (A) are shown. (**C**) The Oct1 and Utx peak lists were intersected (overlap ≥ 1 bp)
510 and plotted as a Venn diagram. 69% of Oct1 peaks overlapped with Utx binding events. (**D**)
511 H3K27me3 ChIP-qPCR enrichment at the *Pax3* promoter in parental and cKO cells at MD

512 differentiation D0 (ESC) and D6. Normalized fold-enrichment is shown relative to both an isotype
513 control antibody and to a nonspecific genomic region encoding the 28S ribosomal subunit. Data
514 represent an average of 3 biological replicates. Error bars depict ±SEM. (**E**) H3K27me3
515 immunofluorescence images from D6 MD-differentiated parental and cKO cultures. Images were
516 collected a 40× magnification. (**F**) Utx enrichment at the *Pax3* promoter in parental and cKO cells
517 on differentiation D6. Fold-enrichment relative to an isotype control antibody and a nonspecific
518 28S region is shown. Data represent an average of 3 independent biological replicates. Error bars
519 depict ±SEM. (**G**) Utx immunoprecipitation followed by Oct1 immunoblot using parental ESCs, or
520 ESCs MD-differentiated for 6D. (**H**) Signal tracks (*Mm10* v.D191020) showing Oct4, Oct1 and Utx
521 enrichment at the *Pax3* locus 5' region. Y-axes were group-autoscaled for each gene. Positions
522 of identified HOMER motifs are shown below.
523
524 **Figure 6. Oct1 and Smad3 cooperate to drive expression of mesoderm-specific genes.** (**A**)
525 HOMER motif analysis of Oct1 peaks that are shared with Oct4 in ESCs, and maintained after D6
526 of MD differentiation. (**B**) Smad3 immunoblot using cell lysates immunoprecipitated with Oct1
527 antibodies, or rabbit IgG controls. D6 MD-differentiated cells were used. 20% input is shown (lane
528 1). (**C**) *Smad3* gene expression is shown in violin plots for parental ESCs at D6 of MD
529 differentiation. (**D**) Scheme for Oct1/Smad reporter assay. A segment of a mouse *Myog* enhancer
530 element containing multiple Oct and Smad motifs was cloned with the core CMV promoter
531 upstream of secreted nLuc and co-transfected into Oct1-deficient MEFs together with a construct
532 encoding constitutive secreted mCherry as a normalization control. Added TGFb1 and co-
533 transfected mouse Oct1 supply Oct1 and Smad3 activity. (**E**) Transfected WT (left panel) or
534 Oct/Smad mutant (right panel) *Myog* enhancer constructs were supplied with Oct1, recombinant
535 purified TGFb1 treatment, or both. Secreted luciferase activity was assessed relative to secreted
536 mCherry expressed from a co-transfected plasmid. An average of experimental triplicates is
537 shown. Error bars denote ±SEM. For the situation in which both Oct1 and TGFb1 are both
538 supplied, fold changes relative to a double-mutant construct are also shown. (**F**) Signal tracks
539 (*Mm10* v. D191020) showing Oct1ChIP-seq enrichment at the *Myog* locus. Shown above are
540 RNA-seq tracks in differentiated and undifferentiated parental and cKO cells. ENCODE-annotated
541 regulatory elements are shown below. Pink: proximal promoter. Yellow: distal enhancer.
542

543 **Figure 7. Sequential model of bivalency resolution for lineage-appropriate (MD-specific)**
544 **genes.** Pluripotent cells co-express Oct1 and Oct4, which co-bind to poised targets. Upon loss of
545 pluripotency and Oct4, Oct1 continues to occupy these genes. TGFβ signals allow co-binding of
546 Oct1 and Smad proteins to MD-specific targets, recruitment of Utx and demethylation of
547 H3K27me3. Later, other transcription factors serve as primary "on" switches for muscle-specific
548 gene expression.

549 **Methods**

550 The datasets generated during this study are available through the GEO website [GSE160941].

551

552 **Cell culture.** ESCs were cultured as previously described (Shakya et al., 2015) with 2i conditions:
553 ERK inhibitor PD0325901 (1 μM, LC Laboratories) and GSK3 inhibitor CHIR99021 (3 μM, LC
554 Laboratories). Cultures were maintained on irradiated feeders (ThermoFisher). Prior to all
555 experiments ESCs were plated on gelatin to deplete the feeders. For Oct1 deletion, cells were
556 treated with 4-hydroxytamoxifen and a completely yellow sub-colony was picked and expanded
557 as published (Shen et al., 2017). For MD differentiation, ESCs were plated on gelatin and cultured
558 as previously described (Chal et al., 2015). Briefly, parental and cKO cells were cultured in N2B27
559 medium supplemented with recombinant Bmp4 (Peprotech) for 2 d. After 48 hr, media was
560 changed to RDL (Rspo3, DMSO, LDN) medium. Cells were harvested 24 hr (day 3) or 96 hr (day
561 6) later. For muscle differentiation, cells were switched to HIFL (Hgf, Igf, Fgf, Ldn) medium and
562 cultured for 48 hr (day 8) after which medium was switched to 2% horse serum (ThermoFisher).
563 Cells were harvested on day 11 (overexpression experiments) or 19 (RT-qPCR).

564

565 **Immunofluorescence.** Immunofluorescence was performed as described previously (Gnocchi et
566 al., 2009) with modifications, using rabbit anti-H3K27me3 (Milipore) and mouse anti-MyHC-emb
567 (eMyHC, Developmental Hybridoma bank) antibodies. Secondary antibodies were goat anti-
568 rabbit-Alexa568 and anti-mouse-Alexa568 (ThermoFisher).

569

570 **Retroviral Oct1 overexpression.** Oct1 was ectopically expressed in ESC cells using a previously
571 described retroviral vector (pBabePuro-Oct1) (Kang et al., 2009b). pBabePuro was used as an
572 empty vector control. The vector was co-transfected together with the pCL-Eco packaging plasmid
573 into HEK293T cells to generate retroviral particles. Retroviral supernatants were collected 48 hr
574 later, filtered through 0.45 μm filters and applied to ESCs cultures maintained on puromycin-
575 resistant feeder fibroblasts (ThermoFisher). The mixed population of cells was subjected to
576 selection with puromycin for 48 hr.

577

578 **RT-qPCR.** RNA was isolated using TRIzol (ThermoFisher). cDNA was synthesized using a
579 SuperScript Vilo cDNA Synthesis Kit (ThermoFisher). RT-qPCR oligonucleotide primers are listed
580 in Supplementary Table 6 and were confirmed to generate a single product of the correct size. To

581 ensure specific PCR amplification, every RT-qPCR run was followed by a dissociation phase
582 analysis (denaturation curve) to confirm the presence of single amplified peaks.
583
584 **Bulk RNA-seq.** RNA was prepared from three independent cultures of undifferentiated or 3 d and
585 6 d MD-differentiated parental or cKO ESCs. Poly(A) RNA was purified from total RNA samples
586 (100–500 ng) with oligo(dT) magnetic beads, and stranded mRNA sequencing libraries were
587 prepared as described using the Illumina TruSeq mRNA library preparation kit and RNA UD
588 Indexes. Molarity of adapter-modified molecules was defined by qPCR using the Kapa
589 Biosystems Library Quant Kit. Individual libraries were normalized to 1.3 nM. Sequencing libraries
590 were chemically denatured and applied to an Illumina NovaSeq flow cell using the NovaSeq XP
591 chemistry workflow. Following transfer of the flowcell to an Illumina NovaSeq instrument, 2×51
592 cycle paired-end sequence was performed using a NovaSeq S1 reagent kit. Between 13 and 18
593 million paired-end reads were generated for each condition. More than 99% of aligned reads
594 mapping to the correct strand.
595
596 **Bulk RNA-seq analysis.** The Illumina adapter sequence was trimmed using cutadapt version
597 1.16. Fastq data quality were checked using Fastqc verision 0.11.5. Reads were aligned to the
598 mouse *Mm10* genome using STAR version 2.7.3a in two-pass mode. Aligned reads were checked
599 for quality using the Picard tools' CollectRnaSeqMetrics command to count the number of read-
600 matching exons, UTRs, introns and intergenic regions, and to calculate normalized gene
601 coverage from the top 1000 expressed transcripts. Between 13 and 18 million paired-end reads
602 were generated for each condition, with >99% of aligned reads mapping to the correct strand.
603 Differentially expressed genes were identified using a 5% FDR with DESeq2 version 1.24.0 (Love
604 et al., 2014). Genes with a count of at least 50 in one or more samples were tested. Genes
605 showing at least 2.5-fold change of expression at an adjusted $p<0.01$ were selected as
606 differentially expressed. Figures were generated in R version 4.0.0 using functions from ggplots
607 libraries and pheatmap.
608
609 **Single-cell RNA-seq.** Single cell transcriptomes were analyzed as described previously
610 (Dell'Orso et al., 2019). The 10X Genomics Chromium Single Cell Gene Expression Solution with
611 3' chemistry, version 3 (PN-1000075) was used to tag individual cells with 16 bp barcodes and
612 specific transcripts with 10 bp Unique Molecular Identifiers (UMIs) according to manufacturer
613 instructions. Briefly, single-cell suspensions were isolated using trypsinization and resuspension

614 in PBS with 0.04% BSA (ThermoFisher). Suspensions were filtered through 40 μm cell strainers.
615 Viability and cell count were assessed using a Countess I (ThermoFisher). Equilibrium to targeted
616 cell recovery of 6,000 cells along with Gel Beads and reverse transcription reagents were loaded
617 to Chromium Single Cell A to form Gel-bead-in Emulsions (GEMs). Within individual GEMs, cDNA
618 generated from captured and barcoded mRNA was synthesized by reverse transcription at 53°C
619 for 45 min. Samples were then heated to 85°C for 5 min. Subsequent A tailing, end repair, adaptor
620 ligation and sample indexing were performed in bulk according to manufacturer instructions. The
621 resulting barcoding libraries were qualified on Agilent Technology 2200 TapeStation system and
622 subjected to qPCR using a KAPA Biosystems Library Quantification Kit for Illumina Platforms
623 (KK4842). The multiple libraries were then normalized and sequenced on an Illumina NovaSeq
624 6000 using the 2×150 PE mode.
625
626 **Single-cell RNA-seq data processing and clustering.** Sequences from the Chromium platform
627 were de-multiplexed and aligned using CellRanger ver. 3.1.0 (10X Genomics) with default
628 parameters mm10-3.0.0. Clustering, filtering, variable gene selection and dimensionality
629 reduction were performed using Seurat ver.3.1.5 (Stuart et al., 2019) according to the following
630 workflow: 1, Cells with <300 detected genes and >10000 genes were excluded further analysis.
631 2, Cells with <12% UMIs mapping to mitochondrial genes were retained for downstream analysis.
632 3, The UMI counts per ten thousand were log-normalized for each cell using the natural logarithm.
633 4, Variable genes (2000 features) were selected using the FindVariableFeatures function. 5,
634 Common anchors between the three parental timepoints (Figure 2A) or parental and cKO D6
635 (Figure 2C) were identified using FindIntegrationAnchors function that were further used to
636 integrate these sets. 6, Gene expression levels in the integrated set were scaled along each gene
637 and linear dimensional reduction was performed. The number of principal components was
638 decided through the assessment of statistical plots (JackStrawPlot and ElbowPlot). 7, Cells were
639 clustered using a by a shared nearest neighbor (SNN) modularity optimization-based clustering
640 algorithm and visualized using two-dimensional uniform manifold approximation and projection
641 (UMAP). 8, Cluster identities were defined based on the distribution of the specific markers.
642 Differentiational gene expression analysis between the parental and cKO clusters was performed
643 using FindMarkers. Genes with adjusted $p<0.01$ were marked red on scatter plots. Using this
644 analysis, the cell numbers were between 1000 and 2500. Reads/cell ranged between 90,000 and
645 200,000. Genes/cell ranged between 2,300 and 7,000. The percentage of reads mapping to

646 reference mouse genome was 90% or higher, and the reads confidently mapping to exonic
647 regions was 70% or higher.
648
649 **Pseudotime and Velocity analysis.** Trajectory analysis of scRNA-seq was performed using
650 Monocle v.2.16.0 (Trapnell et al., 2014). Parental and cKO sets were filtered using the same
651 parameters as above and merged to generate WT and cKO sets. Cells were ordered based on
652 gene lists for the ESC (beginning) and somite (end) clusters in parental UMAP (Figure 2A). Next,
653 we performed dimensional reduction using the DDRTree method to visualize the dataset, ordered
654 the cells by global gene expression levels, and visualized the trajectory of the dataset. Veolocity
655 analysis was performed using the velocyto package (La Manno et al., 2018). Loom files were
656 produced using following paramters: velocyto run10x -m mm10. rmsk.gtf genes.gtf. Gtf files were
657 produced from the Cell Ranger pipeline. Velocity embeddings were produced using the velocyto.r
658 and SeuratWrappers packages. Matrices were filtered using following parameters:
659 nFeature_spliced > 300, nFeature_spliced < 10000, nFeature_unspliced > 200,
660 nFeature_unspliced < 6000, percent.mt < 12. Velocity was calculated using RunVelocity using
661 following paremeters: deltaT = 1, kCells = 25, fit.quantile = 0.02. Velocity embedding were
662 projected on T-SNE maps using the show.velocity.on.embedding.cor function.
663
664 **ChIP.** ChIP-qPCR and ChIP-seq were performed as previously described (Perovanovic et al.,
665 2016). Briefly, WT and cKO cells were crosslinked with 1% formaldehyde for 10 min and
666 quenched for 5 min using 2.5M glycine. Culture plates were washed using ice cold PBS and cells
667 were harvested by cell scaping. Cells were lysed in Farnham buffer (5 mM Pipes pH 8.0, 85 mM
668 KCl, 0.5% NP-40) and subsequently in RIPA buffer (phosphate-buffered saline, 1% NP-40, 0.5%
669 sodium deoxycholate, 0.1% SDS). Chromatin was sheared using a Covaris sonicator for 5 min
670 (30 sec on/30 sec off) with amplitude=40. Correct chromatin fragmentation was confirmed using
671 1% agarose gels. 50 µg of chromatin was subjected to IP overnight at 4°C with 4 µg of anti-Oct1
672 (Novus Biological), Oct4 (Santa Cruz) or H3K27me3 (Milipore) antibodies. As a control, we used
673 5 µg of sheared, non-precipitated input chromatin. Samples were incubated with protein G
674 magnetic beads (ThermoFisher) for 5 hr and washed in Low Salt buffer (20 mM Tris-Cl pH 8.0,
675 150 mM NaCl, 2 mM EDTA, 0.1% SDS, 1% Triton X-100), High Salt buffer (identical but with 500
676 mM NaCl), LiCl buffer, and Tris-EDTA pH 8.0 plus 1 mM EDTA (TE buffer). Washes were
677 performed at 4°C for 10 min with rotation. For re-ChIP, 2% fragmented chromatin was saved as
678 input and the rest used for IP with the primary antibody (either Utx or Oct1) at 4°C overnight on a

679 rotator. Samples were then incubated with magnetic beads for 5h at 4°C. The beads were washed
680 for 10 min with Low Salt buffer, High Salt buffer, Low Salt buffer, LiCl buffer, and TE buffer
681 sequentially at 4°C. Chromatin was eluted with 300 μL IP Elution buffer at RT, then diluted 10-
682 fold in RIPA buffer. Diluted samples were then subjected to a second IP with 4 μg of the secondary
683 antibody (Oct1 or Oct4) at 4°C overnight, and incubated with magnetic beads for 5 hr at 4°C. The
684 beads were washed again as described above, then eluted with 300 μL IP Elution Buffer at RT.
685 Re-ChIP samples, together with the 2% input, were incubated at 65°C overnight to reverse
686 crosslinking. DNA was purified using phenol-chloroform-isoamyl alcohol extraction followed by
687 PCR clean up. qPCR primers can be found in Supplementary Table 6 and were confirmed to
688 generate a single product of the correct size. The results were reported as qPCR values
689 normalized to input chromatin (gDNA) and non-specific region and presented as fold enrichment.
690
691 **ChIP-seq analysis.** After chromatin was precipitated as described above, and libraries were
692 sequenced using Illumina NovaSeq. Between 22 and 26 million paired-end Illumina sequencing
693 reads were aligned to the mouse *Mm10* reference genome using Novocraft novoalign v3.8.2,
694 allowing for one random alignment of multi-mapping reads, and providing the adapter sequences
695 for automatic trimming concordant with alignment. ChIP was analyzed using the
696 MultiRepMacsChIPSeq pipeline v12.2, using options "--pe --optdist 10000 --dupfrac 0.15 --mapq
697 10 --cutoff 2 --tdep 10 --peaksize 500 --peakgap 100 --species mouse --chrskip 'chrMlPhiX' --
698 blacklist mm10.blacklist.bed".
699
700 **Immunoprecipitation.** Cells were lysed with Cell Lysis Buffer (Life Technologies) in the presence
701 of protease inhibitors (EDTA-free tablet, Roche). IP was performed using 500 µg of extract.
702 Extracts were incubated with 4 µg of anti-Utx (Cell Signaling, D3Q1I) or Oct1 (Novus Biologicals,
703 NBP2-21584) antibodies, or rabbit IgG control overnight at 4°C. Protein-antibody complexes were
704 precipitated with protein-G magnetic beads (Thremo Fisher) for 3 hr at 4°C with rotation and
705 washed 3 times with Low Salt buffer (20 mM Tris-HCl pH 8.0, 150 mM NaCl, 2 mM EDTA, 0.1%
706 SDS, 1% Triton X-100) plus protease inhibitors. Precipitated proteins were analyzed by
707 immunoblot.
708
709 **Luciferase reporter assay.** Single or combination mutations were introduced into the Oct1 and
710 Smad consensus binding sites in the following mouse *Myog* regulatory element (*Mm10*
711 chr1:134,285,666-134,285,750). IDT g-blocks® were synthesized to contain WT sequences or

712 single or combined mutations in the Oct1 or Smad binding sites, fused upstream of the CMV basal
713 promoter (-216-13 relative to TSS). G-blocks were inserted using sequence- and ligase-
714 independent cloning (Li and Elledge, 2012) upstream of the coding sequence for a secreted nano-
715 luciferase following digestion of vector pNL2.3 (Promega) using *Eco*RV and *Hind*III. The veracity
716 of the cloned inserts was confirmed by Sanger sequencing. 200 ng of reporter plasmid were co-
717 transfected into Oct1-deficient MEFs (Shakya et al., 2009) in DMEM media lacking phenol red
718 (ThermoFisher) together with 400 ng MMP9-mCherry (Wider and Picard, 2017) in 1000 ng total
719 transfected DNA. Where indicated, 400 ng pBabePuro-Oct1 was included in the transfection mix.
720 pUC18 plasmid comprised the balance of the transfected DNA. Where indicated, transfected cells
721 were provided with 5 ng recombinant mouse TGFb1 protein (R&D Systems). mCherry
722 fluorescence was determined first by exciting at 570 nm and measuring emission at 610 nm with
723 a 100 msec time delay using an Envision Xcite Multilabel Plate Reader. Luminescence was
724 measured using Nano-Glo Luciferase (Promega) and a Modulus luminescence plate reader.
725
726 **Metabolic profiling.** Cold 90% methanol (MeOH) was added to each sample to give a final
727 concentration of 80%. Samples were then incubated at -20˚C for 1 hr. After incubation the
728 samples were centrifuged at 20,000×*g* for 10 min at 4˚C. The supernatant was then transferred
729 from each sample tube into a labeled, fresh micro centrifuge tube. Pooled quality control samples
730 were made by removing a fraction of collected supernatant from each sample and process blanks
731 were made using only extraction solvent and no cell culture. The samples were then dried en
732 vacuo. GC-MS was performed with an Agilent 5977b GC-MS MSD-HES and an Agilent 7693A
733 automatic liquid sampler. Data were analyzed using in-house software to prepare for analysis by
734 the "MetaboAnalyst" software tool (Chong et al., 2018). Statistical analysis was performed using
735 MetaboAnalystR.

Acknowledgements

We thank G. Kardon and C. Kikani for critical reading of the manuscript. We thank B. Dalley and O. Allen at the HCI High-Throughput Genomics facility and T. Parnell and B. Lohman at the HCI Bioinformatic Analysis Shared Resource for assistance with ChIP-seq and scRNA-seq. We thank James E. Cox and Tyler Van Ry from the Metabolomics Core for their assistance with metabolomic profiling. We thank Olivier Pourquié from the Harvard Medical School for the assistance with the mesodermal differentiation protocols. We thank D. Picard and D. Wider for the MMP9-mCherry construct. This work was supported by a grant from the National Institutes of Health/National Institute of General Medical Sciences (R01GM122778) to DT.

Author contributions: DT conceived the study, and provided administrative and material support. JP conceived and supervised experiments, designed experiments and acquired and interpreted data. YW, ZS acquired and interpreted data. MBC generated reagents and analyzed data. All authors were involved in writing, reviewing and revising the manuscript.

Conflict of interest

The authors declare that they have no conflicts of interest

752 **REFERENCES**

753

754 Abascal F, Acosta R, Addleman NJ, Adrian J, Afzal V, Aken B, Akiyama JA, Jammal O Al,
755 Amrhein H, Anderson SM, Andrews GR, Antoshechkin I, Ardlie KG, Armstrong J, Astley M,
756 Banerjee B, Barkal AA, Barnes IHA, Barozzi I, Barrell D, Barson G, Bates D, Baymuradov
757 UK, Bazile C, Beer MA, Beik S, Bender MA, Bennett R, Bouvrette LPB, Bernstein BE,
758 Berry A, Bhaskar A, Bignell A, Blue SM, Bodine DM, Boix C, Boley N, Borrman T, Borsari
759 B, Boyle AP, Brandsmeier LA, Breschi A, Bresnick EH, Brooks JA, Buckley M, Burge CB,
760 Byron R, Cahill E, Cai L, Cao L, Carty M, Castanon RG, Castillo A, Chaib H, Chan ET,
761 Chee DR, Chee S, Chen Hao, Chen Huaming, Chen JY, Chen S, Cherry JM, Chhetri SB,
762 Choudhary JS, Chrast J, Chung D, Clarke D, Cody NAL, Coppola CJ, Coursen J, D'Ippolito
763 AM, Dalton S, Danyko C, Davidson C, Davila-Velderrain J, Davis CA, Dekker J, Deran A,
764 DeSalvo G, Despacio-Reyes G, Dewey CN, Dickel DE, Diegel M, Diekhans M, Dileep V,
765 Ding B, Djebali S, Dobin A, Dominguez D, Donaldson S, Drenkow J, Dreszer TR, Drier Y,
766 Duff MO, Dunn D, Eastman C, Ecker JR, Edwards MD, El-Ali N, Elhajjajy SI, Elkins K, Emili
767 A, Epstein CB, Evans RC, Ezkurdia I, Fan K, Farnham PJ, Farrell NP, Feingold EA,
768 Ferreira AM, Fisher-Aylor K, Fitzgerald S, Flicek P, Foo CS, Fortier K, Frankish A, Freese
769 P, Fu S, Fu XD, Fu Y, Fukuda-Yuzawa Y, Fulciniti M, Funnell APW, Gabdank I, Galeev T,
770 Gao M, Giron CG, Garvin TH, Gelboin-Burkhart CA, Georgolopoulos G, Gerstein MB,
771 Giardine BM, Gifford DK, Gilbert DM, Gilchrist DA, Gillespie S, Gingeras TR, Gong P,
772 Gonzalez A, Gonzalez JM, Good P, Goren A, Gorkin DU, Graveley BR, Gray M, Greenblatt
773 JF, Griffiths E, Groudine MT, Grubert F, Gu M, Guigó R, Guo H, Guo Yu, Guo Yuchun,
774 Gursoy G, Gutierrez-Arcelus M, Halow J, Hardison RC, Hardy M, Hariharan M, Harmanci
775 A, Harrington A, Harrow JL, Hashimoto TB, Hasz RD, Hatan M, Haugen E, Hayes JE, He
776 P, He Y, Heidari N, Hendrickson D, Heuston EF, Hilton JA, Hitz BC, Hochman A, Holgren
777 C, Hou L, Hou S, Hsiao YHE, Hsu S, Huang H, Hubbard TJ, Huey J, Hughes TR, Hunt T,
778 Ibarrientos S, Issner R, Iwata M, Izuogu O, Jaakkola T, Jameel N, Jansen C, Jiang L, Jiang
779 P, Johnson A, Johnson R, Jungreis I, Kadaba M, Kasowski M, Kasparian M, Kato M, Kaul
780 R, Kawli T, Kay M, Keen JC, Keles S, Keller CA, Kelley D, Kellis M, Kheradpour P, Kim
781 DS, Kirilusha A, Klein RJ, Knoechel B, Kuan S, Kulik MJ, Kumar S, Kundaje A, Kutyavin T,
782 Lagarde J, Lajoie BR, Lambert NJ, Lazar J, Lee AY, Lee D, Lee E, Lee JW, Lee K, Leslie
783 CS, Levy S, Li B, Li H, Li N, Li X, Li YI, Li Ying, Li Yining, Li Yue, Lian J, Libbrecht MW, Lin
784 S, Lin Y, Liu D, Liu J, Liu P, Liu T, Liu XS, Liu Yan, Liu Yaping, Long M, Lou S, Loveland J,

785 Lu A, Lu Y, Lécuyer E, Ma L, Mackiewicz M, Mannion BJ, Mannstadt M, Manthravadi D,
786 Marinov GK, Martin FJ, Mattei E, McCue K, McEown M, McVicker G, Meadows SK,
787 Meissner A, Mendenhall EM, Messer CL, Meuleman W, Meyer C, Miller S, Milton MG,
788 Mishra T, Moore DE, Moore HM, Moore JE, Moore SH, Moran J, Mortazavi A, Mudge JM,
789 Munshi N, Murad R, Myers RM, Nandakumar V, Nandi P, Narasimha AM, Narayanan AK,
790 Naughton H, Navarro FCP, Navas P, Nazarovs J, Nelson J, Neph S, Neri FJ, Nery JR,
791 Nesmith AR, Newberry JS, Newberry KM, Ngo V, Nguyen R, Nguyen TB, Nguyen T,
792 Nishida A, Noble WS, Novak CS, Novoa EM, Nuñez B, O'Donnell CW, Olson S, Onate KC,
793 Otterman E, Ozadam H, Pagan M, Palden T, Pan X, Park Y, Partridge EC, Paten B, Pauli-
794 Behn F, Pazin MJ, Pei B, Pennacchio LA, Perez AR, Perry EH, Pervouchine DD, Phalke
795 NN, Pham Q, Phanstiel DH, Plajzer-Frick I, Pratt GA, Pratt HE, Preissl S, Pritchard JK,
796 Pritykin Y, Purcaro MJ, Qin Q, Quinones-Valdez G, Rabano I, Radovani E, Raj A,
797 Rajagopal N, Ram O, Ramirez L, Ramirez RN, Rausch D, Raychaudhuri S, Raymond J,
798 Razavi R, Reddy TE, Reimonn TM, Ren B, Reymond A, Reynolds A, Rhie SK, Rinn J,
799 Rivera M, Rivera-Mulia JC, Roberts BS, Rodriguez JM, Rozowsky J, Ryan R, Rynes E,
800 Salins DN, Sandstrom R, Sasaki T, Sathe S, Savic D, Scavelli A, Scheiman J, Schlaffner
801 C, Schloss JA, Schmitges FW, See LH, Sethi A, Setty M, Shafer A, Shan S, Sharon E,
802 Shen Q, Shen Y, Sherwood RI, Shi M, Shin S, Shoresh N, Siebenthall K, Sisu C, Slifer T,
803 Sloan CA, Smith A, Snetkova V, Snyder MP, Spacek D V., Srinivasan S, Srivas R,
804 Stamatoyannopoulos G, Stamatoyannopoulos JA, Stanton R, Steffan D, Stehling-Sun S,
805 Strattan JS, Su A, Sundararaman B, Suner MM, Syed T, Szynkarek M, Tanaka FY, Tenen
806 D, Teng M, Thomas JA, Toffey D, Tress ML, Trout DE, Trynka G, Tsuji J, Upchurch SA,
807 Ursu O, Uszczynska-Ratajczak B, Uziel MC, Valencia A, Biber B Van, van der Velde AG,
808 Van Nostrand EL, Vaydylevich Y, Vazquez J, Victorsen A, Vielmetter J, Vierstra J, Visel A,
809 Vlasova A, Vockley CM, Volpi S, Vong S, Wang H, Wang M, Wang Q, Wang R, Wang T,
810 Wang W, Wang X, Wang Y, Watson NK, Wei X, Wei Z, Weisser H, Weissman SM, Welch
811 R, Welikson RE, Weng Z, Westra HJ, Whitaker JW, White C, White KP, Wildberg A,
812 Williams BA, Wine D, Witt HN, Wold B, Wolf M, Wright J, Xiao R, Xiao X, Xu J, Yan KK,
813 Yan Y, Yang H, Yang X, Yang YW, Yardimci GG, Yee BA, Yeo GW, Young T, Yu T, Yue F,
814 Zaleski C, Zang C, Zeng H, Zeng W, Zerbino DR, Zhai J, Zhan L, Zhan Y, Zhang B, Zhang
815 Jialing, Zhang Jing, Zhang K, Zhang L, Zhang P, Zhang Q, Zhang XO, Zhang Y, Zhang Z,
816 Zhao Y, Zheng Y, Zhong G, Zhou XQ, Zhu Y, Zimmerman J. 2020. Expanded
817 encyclopaedias of DNA elements in the human and mouse genomes. *Nature* **583**:699–710.

818 doi:10.1038/s41586-020-2493-4
819 Bain G, Kitchens D, Yao M, Huettner JE, Gottlieb DI. 1995. Embryonic stem cells express
820 neuronal properties in vitro. *Dev Biol* **168**:342–357. doi:10.1006/dbio.1995.1085
821 Beddington RSP, Robertson EJ. 1989. An assessment of the developmental potential of
822 embryonic stem cells in the midgestation mouse embryo. *Development* **105**:733–737.
823 Bernstein BE, Mikkelsen TS, Xie X, Kamal M, Huebert DJ, Cuff J, Fry B, Meissner A, Wernig M,
824 Plath K, Jaenisch R, Wagschal A, Feil R, Schreiber SL, Lander ES. 2006. A bivalent
825 chromatin structure marks key developmental genes in embryonic stem cells. *Cell*
826 **125**:315–26. doi:10.1016/j.cell.2006.02.041
827 Chal J, Oginuma M, Tanoury Z Al, Gobert B, Sumara O, Hick A, Bousson F, Zidouni Y, Mursch
828 C, Moncuquet P, Tassy O, Vincent S, Miyanari A, Bera A, Garnier J, Guevara G, Hestin M,
829 Kennedy L, Hayashi S, Drayton B, Cherrier T, Gayraud-morel B, Gussoni E, Relaix F,
830 Tajbakhsh S, Pourquié O. 2015. Differentiation of pluripotent stem cells to muscle fiber to
831 model Duchenne muscular dystrophy. *Nat Biotechnol* **33**:962–9. doi:10.1038/nbt.3297
832 Chong J, Soufan O, Li C, Caraus I, Li S, Bourque G, Wishart DS, Xia J. 2018. MetaboAnalyst
833 4.0: Towards more transparent and integrative metabolomics analysis. *Nucleic Acids Res*
834 **46**:W486–W494. doi:10.1093/nar/gky310
835 Cloos PAC, Christensen J, Agger K, Helin K. 2008. Erasing the methyl mark: Histone
836 demethylases at the center of cellular differentiation and disease. *Genes Dev*.
837 doi:10.1101/gad.1652908
838 Collinson A, Collier AJ, Morgan NP, Sienerth AR, Chandra T, Andrews S, Rugg-Gunn PJ. 2016.
839 Deletion of the Polycomb-Group Protein EZH2 Leads to Compromised Self-Renewal and
840 Differentiation Defects in Human Embryonic Stem Cells. *Cell Rep*.
841 doi:10.1016/j.celrep.2016.11.032
842 Conlon FL, Lyons KM, Takaesu N, Barth KS, Kispert A, Herrmann B, Robertson EJ. 1994. A
843 primary requirement for nodal in the formation and maintenance of the primitive streak in
844 the mouse. *Trends Genet* **10**:308–308. doi:10.1016/0168-9525(94)90026-4
845 Dell'Orso S, Juan AH, Ko K-D, Naz F, Perovanovic J, Gutierrez-Cruz G, Feng X, Sartorelli V.
846 2019. Correction: Single cell analysis of adult mouse skeletal muscle stem cells in
847 homeostatic and regenerative conditions (doi: 10.1242/dev.174177). *Development*
848 **146**:dev181743. doi:10.1242/dev.181743
849 DeVeale B, Brokhman I, Mohseni P, Babak T, Yoon C, Lin A, Onishi K, Tomilin A, Pevny L,
850 Zandstra PW, Nagy A, van der Kooy D. 2013. Oct4 is required ~E7.5 for proliferation in the

851 primitive streak. *PLoS Genet* **9**. doi:10.1371/JOURNAL.PGEN.1003957
852 Dhar SS, Lee SH, Chen K, Zhu G, Oh WK, Allton K, Gafni O, Kim YZ, Tomoiga AS, Barton MC,
853 Hanna JH, Wang Z, Li W, Lee MG. 2016a. An essential role for UTX in resolution and
854 activation of bivalent promoters. *Nucleic Acids Res* **44**:3659–3674.
855 doi:10.1093/nar/gkv1516
856 Dhar SS, Lee SH, Chen K, Zhu G, Oh WK, Allton K, Gafni O, Kim YZ, Tomoiga AS, Barton MC,
857 Hanna JH, Wang Z, Li W, Lee MG. 2016b. An essential role for UTX in resolution and
858 activation of bivalent promoters. *Nucleic Acids Res* **44**:3659–3674.
859 doi:10.1093/nar/gkv1516
860 Diaz-Cuadros M, Wagner DE, Budjan C, Hubaud A, Tarazona OA, Donelly S, Michaut A, Al
861 Tanoury Z, Yoshioka-Kobayashi K, Niino Y, Kageyama R, Miyawaki A, Touboul J,
862 Pourquié O. 2020. In vitro characterization of the human segmentation clock. *Nature*
863 **580**:113–118. doi:10.1038/s41586-019-1885-9
864 Gnocchi VF, White RB, Ono Y, Ellis JA, Zammit PS. 2009. Further characterisation of the
865 molecular signature of quiescent and activated mouse muscle satellite cells. *PLoS One*
866 **4**:e5205. doi:10.1371/journal.pone.0005205
867 Guibentif C, Griffiths JA, Imaz-Rosshandler I, Ghazanfar S, Nichols J, Wilson V, Göttgens B,
868 Marioni JC. 2021. Diverse Routes toward Early Somites in the Mouse Embryo. *Dev Cell*
869 **56**:141-153.e6. doi:10.1016/j.devcel.2020.11.013
870 Heinz S, Benner C, Spann N, Bertolino E, Lin YC, Laslo P, Cheng JX, Murre C, Singh H, Glass
871 CK. 2010. Simple Combinations of Lineage-Determining Transcription Factors Prime cis-
872 Regulatory Elements Required for Macrophage and B Cell Identities. *Mol Cell* **38**:576–589.
873 doi:10.1016/j.molcel.2010.05.004
874 Hnisz D, Abraham BJ, Lee TI, Lau A, Saint-André V, Sigova AA, Hoke HA, Young RA. 2013.
875 Super-enhancers in the control of cell identity and disease. *Cell* **155**:934–47.
876 doi:10.1016/j.cell.2013.09.053
877 Kang J, Gemberling M, Nakamura M, Whitby FG, Handa H, Fairbrother WG, Tantin D. 2009a. A
878 general mechanism for transcription regulation by Octl and Oct4 in response to genotoxic
879 and oxidative stress. *Genes Dev* **23**:208–222. doi:10.1101/gad.1750709
880 Kang J, Gemberling M, Nakamura M, Whitby FG, Handa H, Fairbrother WG, Tantin D. 2009b. A
881 general mechanism for transcription regulation by Oct1 and Oct4 in response to genotoxic
882 and oxidative stress. *Genes Dev* **23**:208–222. doi:10.1101/gad.1750709
883 Ku M, Koche RP, Rheinbay E, Mendenhall EM, Endoh M, Mikkelsen TS, Presser A, Nusbaum

884 C, Xie X, Chi AS, Adli M, Kasif S, Ptaszek LM, Cowan CA, Lander ES, Koseki H, Bernstein
885 BE. 2008. Genomewide Analysis of PRC1 and PRC2 Occupancy Identifies Two Classes of
886 Bivalent Domains. *PLoS Genet* **4**:e1000242. doi:10.1371/journal.pgen.1000242
887 La Manno G, Soldatov R, Zeisel A, Braun E, Hochgerner H, Petukhov V, Lidschreiber K, Kastriti
888 ME, Lönnerberg P, Furlan A, Fan J, Borm LE, Liu Z, van Bruggen D, Guo J, He X, Barker
889 R, Sundström E, Castelo-Branco G, Cramer P, Adameyko I, Linnarsson S, Kharchenko P
890 V. 2018. RNA velocity of single cells. *Nature* **560**:494–498. doi:10.1038/s41586-018-0414-
891 6
892 Lachmann A, Xu H, Krishnan J, Berger SI, Mazloom AR, Ma'ayan A. 2010. ChEA: Transcription
893 factor regulation inferred from integrating genome-wide ChIP-X experiments.
894 *Bioinformatics* **26**:2438–2444. doi:10.1093/bioinformatics/btq466
895 Li MZ, Elledge SJ. 2012. SLIC: A method for sequence- and ligation-independent cloning.
896 *Methods Mol Biol* **852**:51–59. doi:10.1007/978-1-61779-564-0_5
897 Liu Z, Lin X, Cai Z, Zhang Z, Han C, Jia S, Meng A, Wang Q. 2011. Global identification of
898 SMAD2 target genes reveals a role for multiple co-regulatory factors in zebrafish early
899 gastrulas. *J Biol Chem* **286**:28520–28532. doi:10.1074/jbc.M111.236307
900 Love MI, Huber W, Anders S. 2014. Moderated estimation of fold change and dispersion for
901 RNA-seq data with DESeq2. *Genome Biol* **15**:550. doi:10.1186/s13059-014-0550-8
902 McLean CY, Bristor D, Hiller M, Clarke SL, Schaar BT, Lowe CB, Wenger AM, Bejerano G.
903 2010. GREAT improves functional interpretation of cis-regulatory regions. *Nat Biotechnol*
904 **28**:495–501. doi:10.1038/nbt.1630
905 Meshorer E, Misteli T. 2006. Chromatin in pluripotent embryonic stem cells and differentiation.
906 *Nat Rev Mol Cell Biol* **7**:540–6. doi:10.1038/nrm1938
907 Mullen AC, Orlando DA, Newman JJ, Lovén J, Kumar RM, Bilodeau S, Reddy J, Guenther MG,
908 DeKoter RP, Young RA. 2011. Master transcription factors determine cell-type-specific
909 responses to TGF-β signaling. *Cell* **147**:565–76. doi:10.1016/j.cell.2011.08.050
910 Nichols J, Zevnik B, Anastassiadis K, Niwa H, Klewe-Nebenius D, Chambers I, Schöler H,
911 Smith A. 1998. Formation of pluripotent stem cells in the mammalian embryo depends on
912 the POU transcription factor Oct4. *Cell* **95**:379–391. doi:10.1016/S0092-8674(00)81769-9
913 Oginuma M, Moncuquet P, Xiong F, Karoly E, Chal J, Guevorkian K, Pourquié O. 2017. A
914 Gradient of Glycolytic Activity Coordinates FGF and Wnt Signaling during Elongation of the
915 Body Axis in Amniote Embryos. *Dev Cell* **40**:342-353.e10.
916 doi:10.1016/j.devcel.2017.02.001

917 Palmieri SL, Peter W, Hess H, Schöler HR. 1994. Oct-4 transcription factor is differentially
918 expressed in the mouse embryo during establishment of the firsttwo extraembryonic cell
919 lineages involved in implantation. *Dev Biol* **166**:259–267. doi:10.1006/dbio.1994.1312
920 Perovanovic J, DellOrso S, Gnochi VF, Jaiswal JK, Sartorelli V, Vigouroux C, Mamchaoui K,
921 Mouly V, Bonne G, Hoffman EP. 2016. Laminopathies disrupt epigenomic developmental
922 programs and cell fate. *Sci Transl Med* **8**:335ra58-335ra58.
923 doi:10.1126/scitranslmed.aad4991
924 Schlesinger S, Meshorer E. 2019. Open Chromatin, Epigenetic Plasticity, and Nuclear
925 Organization in Pluripotency. *Dev Cell*. doi:10.1016/j.devcel.2019.01.003
926 Sebastiano V, Dalvai M, Gentile L, Schubart K, Sutter J, Wu GM, Tapia N, Esch D, Ju JY,
927 Hübner K, Bravo MJA, Schöler HR, Cavaleri F, Matthias P. 2010. Oct1 regulates
928 trophoblast development during early mouse embryogenesis. *Development* **137**:3551–
929 3560. doi:10.1242/dev.047027
930 Seydoux G, Braun RE. 2006. Pathway to Totipotency: Lessons from Germ Cells. *Cell*.
931 doi:10.1016/j.cell.2006.11.016
932 Shakya A, Callister C, Goren A, Yosef N, Garg N, Khoddami V, Nix D, Regev A, Tantin D. 2015.
933 Pluripotency transcription factor Oct4 mediates stepwise nucleosome demethylation and
934 depletion. *Mol Cell Biol* **35**:1014–25. doi:10.1128/MCB.01105-14
935 Shakya A, Cooksey R, Cox JE, Wang V, McClain DA, Tantin D. 2009. Oct1 loss of function
936 induces a coordinate metabolic shift that opposes tumorigenicity. *Nat Cell Biol* **11**:320–327.
937 doi:10.1038/ncb1840
938 Shakya A, Kang J, Chumley J, Williams MA, Tantin D. 2011. Oct1 is a switchable, bipotential
939 stabilizer of repressed and inducible transcriptional states. *J Biol Chem* **286**:450–9.
940 doi:10.1074/jbc.M110.174045
941 Shen Z, Kang J, Shakya A, Tabaka M, Jarboe EA, Regev A, Tantin D. 2017. Enforcement of
942 developmental lineage specificity by transcription factor Oct1. *Elife* **6**.
943 doi:10.7554/eLife.20937
944 Stuart T, Butler A, Hoffman P, Hafemeister C, Papalexi E, Mauck WM, Hao Y, Stoeckius M,
945 Smibert P, Satija R. 2019. Comprehensive Integration of Single-Cell Data. *Cell* **177**:1888-
946 1902.e21. doi:10.1016/j.cell.2019.05.031
947 Takahashi K, Yamanaka S. 2006. Induction of Pluripotent Stem Cells from Mouse Embryonic
948 and Adult Fibroblast Cultures by Defined Factors. *Cell* **126**:663–676.
949 doi:10.1016/j.cell.2006.07.024

950 Tantin D. 2013. Oct transcription factors in development and stem cells: insights and
951 mechanisms. *Development* **140**:2857–2866. doi:10.1242/dev.095927
952 Tantin D, Schild-Poulter C, Wang V, Haché RJG, Sharp PA. 2005. The Octamer Binding
953 Transcription Factor Oct-1 Is a Stress Sensor. *Cancer Res* **65**:10750–10758.
954 doi:10.1158/0008-5472.CAN-05-2399
955 Trapnell C, Cacchiarelli D, Grimsby J, Pokharel P, Li S, Morse M, Lennon NJ, Livak KJ,
956 Mikkelsen TS, Rinn JL. 2014. The dynamics and regulators of cell fate decisions are
957 revealed by pseudotemporal ordering of single cells. *Nat Biotechnol* **32**:381–386.
958 doi:10.1038/nbt.2859
959 Wang C, Lee JE, Cho YW, Xiao Y, Jin Q, Liu C, Ge K. 2012. UTX regulates mesoderm
960 differentiation of embryonic stem cells independent of H3K27 demethylase activity. *Proc*
961 *Natl Acad Sci U S A* **109**:15324–15329. doi:10.1073/pnas.1204166109
962 Wang V. E. H., Schmidt T, Chen J, Sharp PA, Tantin D. 2004. Embryonic Lethality, Decreased
963 Erythropoiesis, and Defective Octamer-Dependent Promoter Activation in Oct-1-Deficient
964 Mice. *Mol Cell Biol* **24**:1022–1032. doi:10.1128/mcb.24.3.1022-1032.2004
965 Wang Victoria E. H., Schmidt T, Chen J, Sharp PA, Tantin D. 2004. Embryonic lethality,
966 decreased erythropoiesis, and defective octamer-dependent promoter activation in Oct-1-
967 deficient mice. *Mol Cell Biol* **24**:1022–1032. doi:10.1128/MCB.24.3.1022-1032.2004
968 Wider D, Picard D. 2017. Secreted dual reporter assay with Gaussia luciferase and the red
969 fluorescent protein mCherry. *PLoS One* **12**:e0189403. doi:10.1371/journal.pone.0189403
970 Zhang Y, Lahmann I, Baum K, Shimojo H, Mourikis P, Wolf J, Kageyama R, Birchmeier C.
971 2021. Oscillations of Delta-like1 regulate the balance between differentiation and
972 maintenance of muscle stem cells. *Nat Commun* **12**. doi:10.1038/s41467-021-21631-4
973 Zhou X, Sasaki H, Lowe L, Hogan BLM, Kuehn MR. 1993. Nodal is a novel TGF-β-like gene
974 expressed in the mouse node during gastrulation. *Nature* **361**:543–547.
975 doi:10.1038/361543a0
976

Perovanovic *et al.* Figure 1

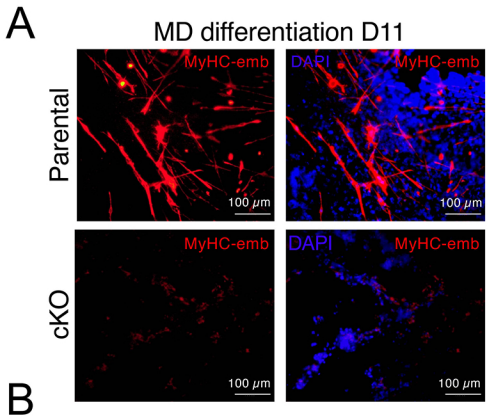

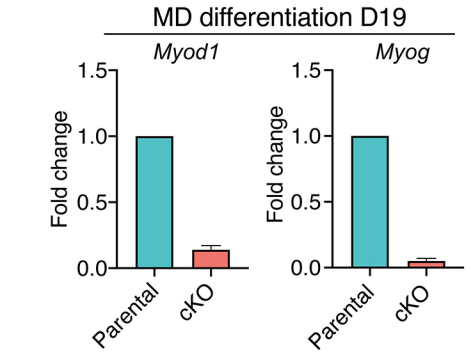

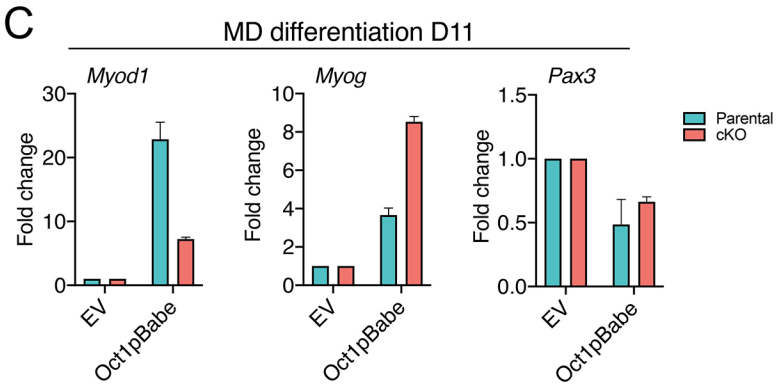

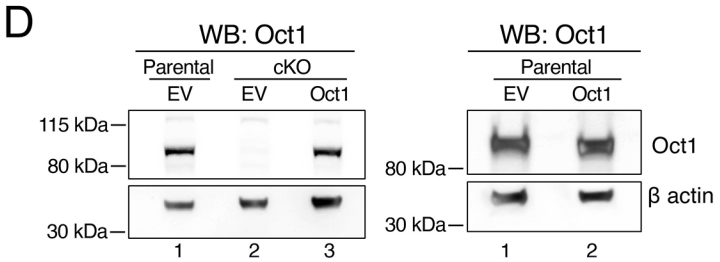

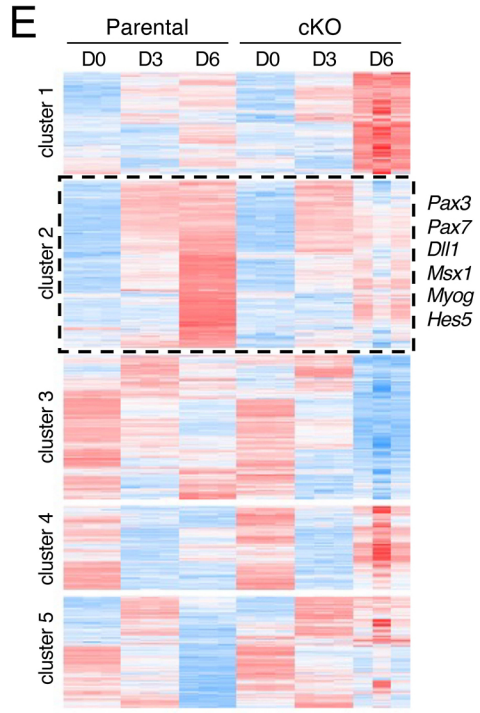

F

Cluster 1 Enrichment

Jensen Tissue	Adj. *p*-value
Germ cell	2.8E-6
Primordium	1.5E-5

Cluster 2 Enrichment

Jensen Tissue	Adj. *p*-value
Neural Tube	2.8E-6
Somite	3.8E-5

Cluster 2 Regulation

ChEA 2016	Adj. *p*-value
SUZ12	1.836E-21
MTF2	7.127E-21
JARID2	2.807E-20
EZH2	7.379E-20

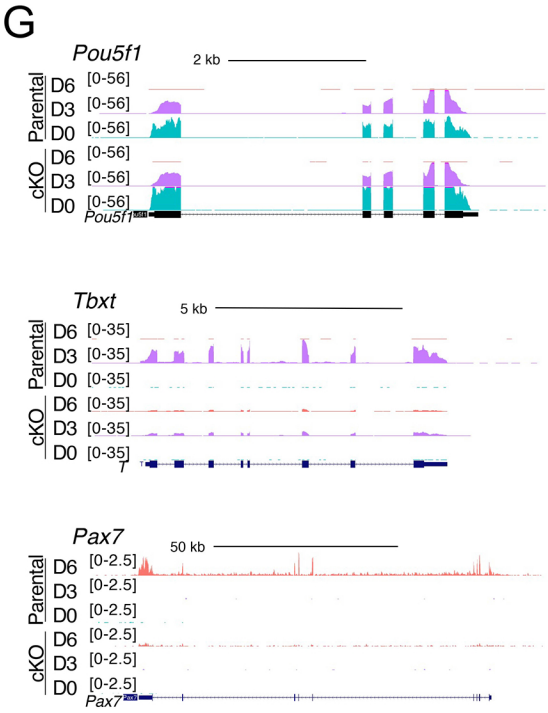

Perovanovic *et al.* Figure 2

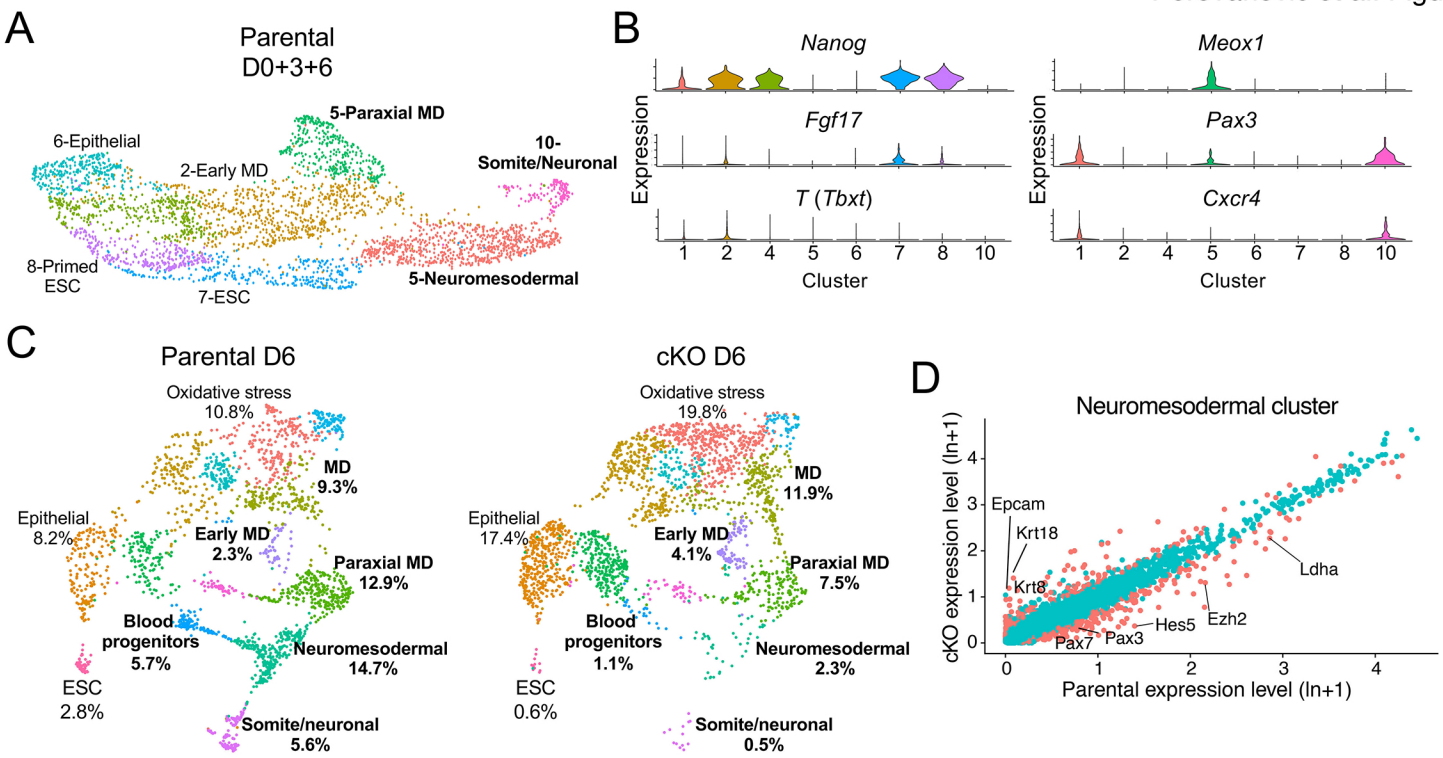

Perovanovic *et al.* Figure 3

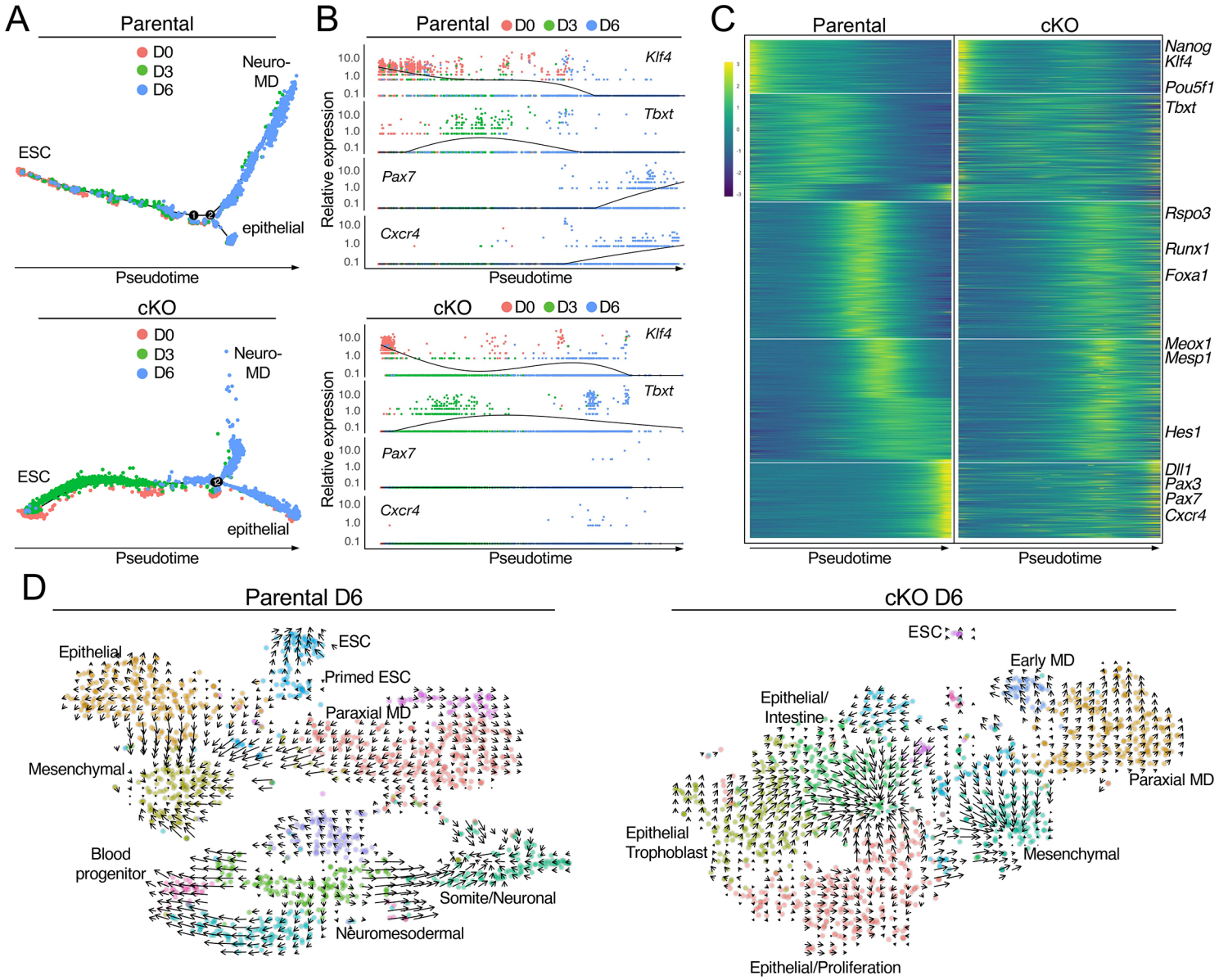

Perovanovic *et al.* Figure 4

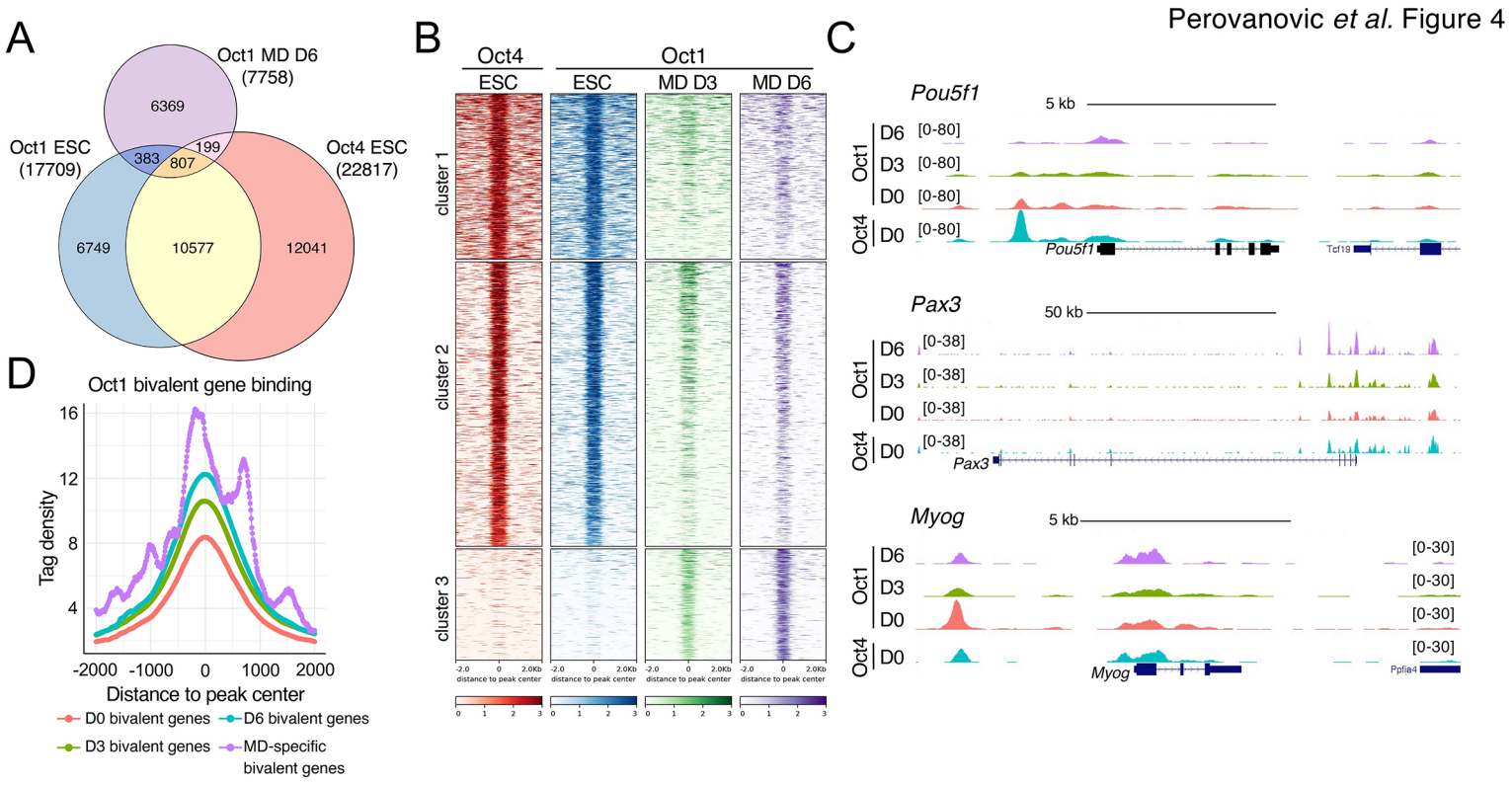

Perovanovic *et al.* Figure 5

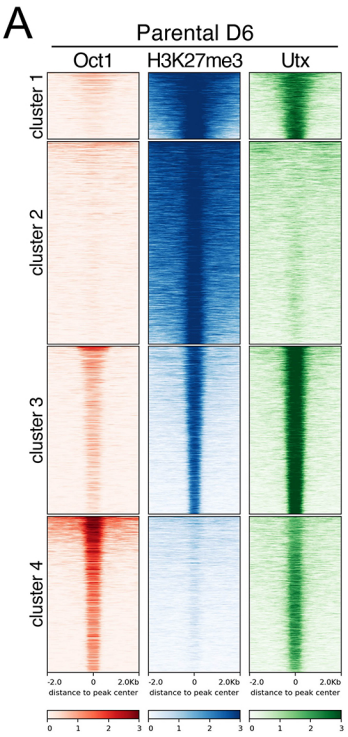

B

Cluster 3 Enrichment

Human Phenotype Ontology	Binome FDR
Abnormality of the musculature	2.00E-46
Abnormality of muscle physiology	1.20E-44
Abnormality of skeleton morphology	7.51E-41

Cluster 4 Enrichment

Human Phenotype Ontology	Binome FDR
Abnormality of the musculature	1.99E-39
Global developmental delay	1.72E-36
Neurodevelopmental delay	2.82E-35
Abnormality of metabolism	5.28E-35

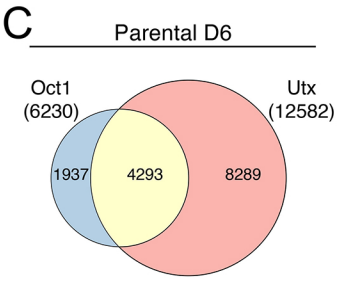

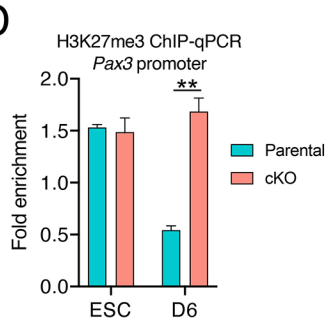

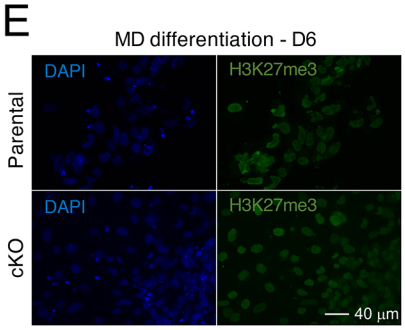

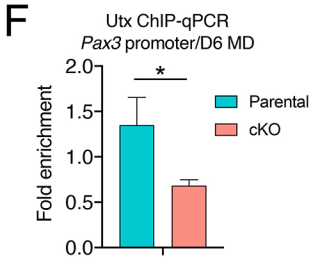

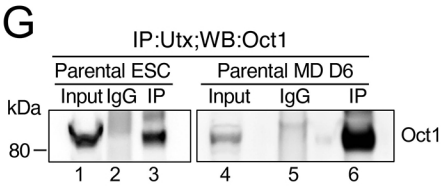

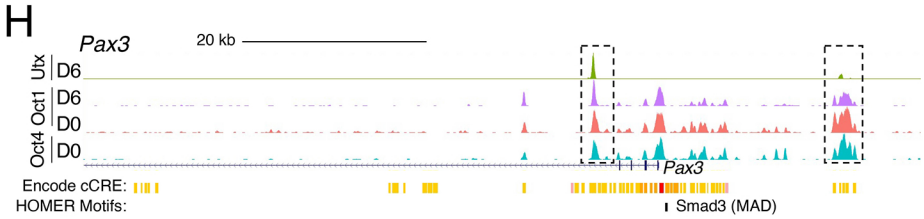

Perovanovic *et al.* Figure 6

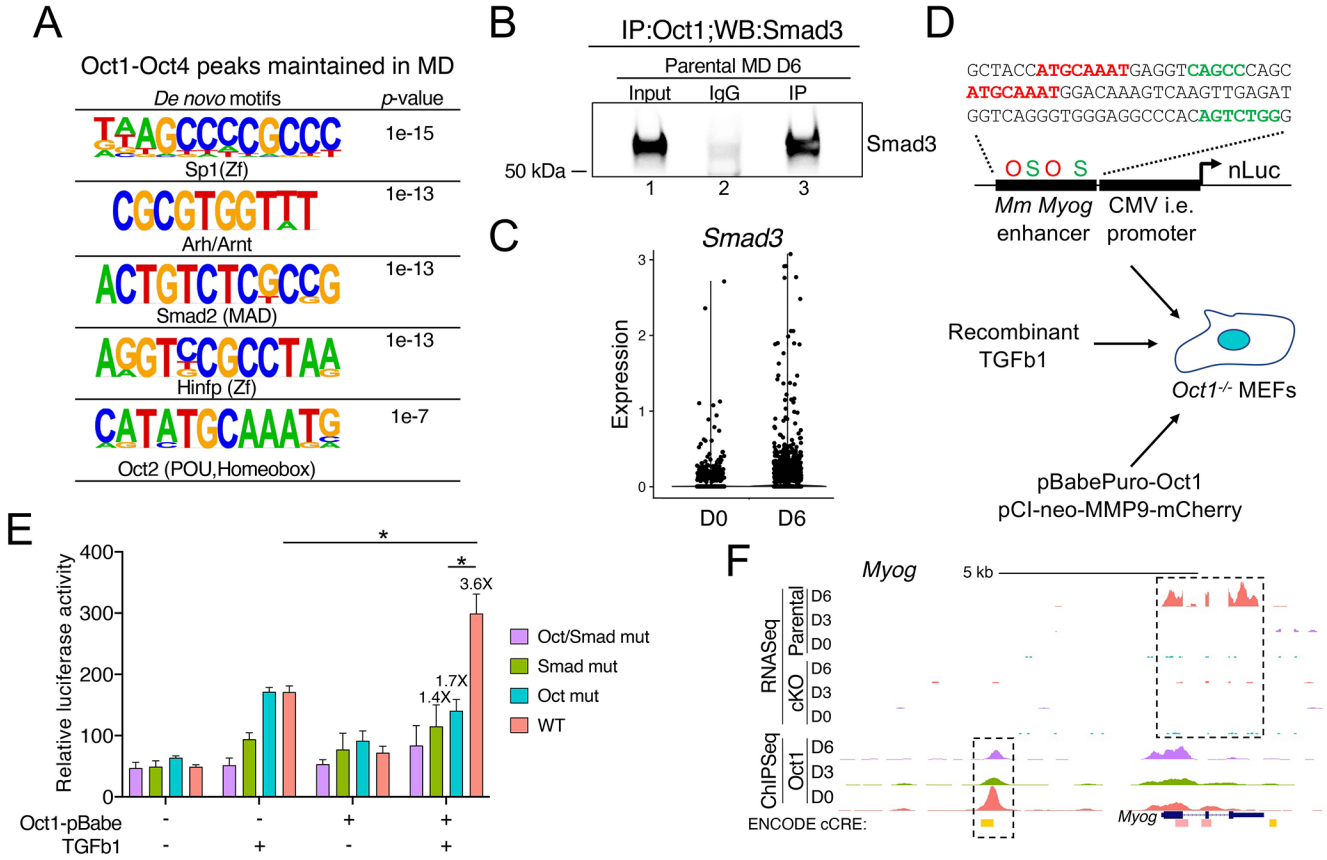
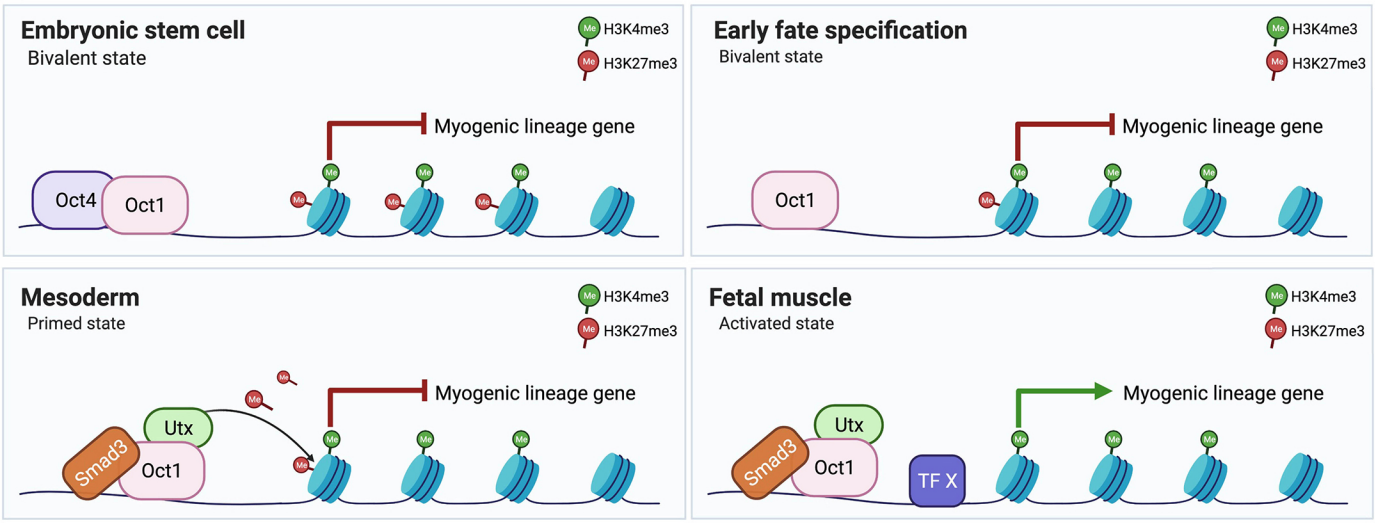
Perovanovic *et al.* Figure 7